ACS APPLIED BIO MATERIALS

www.acsabm.org Review

Recent Progress in Cellulose Nanocrystal Alignment and Its Applications

Ragesh Prathapan, Rico F. Tabor, Gil Garnier, and Jinguang Hu*

Cite This: *ACS Appl. Bio Mater.* 2020, 3, 1828−1844 Read Online

ACCESS | Metrics & More | Article Recommendations

ABSTRACT: Cellulose nanocrystal (CNC) research has addressed increased attention in the bioprocessing community, especially the utility of these materials in different fields, including biomedical and materials applications. In this review, the different preparation methods and properties of CNC materials will be initially briefly discussed. The latter focuses special attention on the alignment of CNCs and its applications. Different methods to induce CNC alignment, including self-assembly, shear-based alignment, magnetic and electric field alignment, spin-coating, dip-coating, etc., are reviewed in detail, followed by the different characterization techniques to quantify the alignments of CNCs. The current and potential applications of aligned CNCs, such as fillers to enhance the mechanical and thermal properties of biocomposites, photonic materials to deal with structural colors and enhancement in optical properties of iridescent films, and reduced wettability for high-resolution printing, are further discussed to provide more insights into this promising research direction. We hope that this review will shine light on CNC alignment and also open the door to different types of applications.

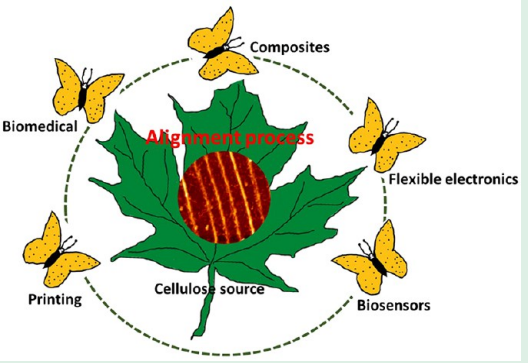

KEYWORDS: *cellulose nanocrystals, CNC preparation, CNC alignment, alignment characterization, alignment applications, wrinkling*

1. INTRODUCTION

Concerns about increasing levels of carbon emissions, global warming, and energy security have encouraged governments around the world to gradually shift from the traditional hydrocarbon based "oil refinery" to the sustainable carbohydrate-based "biorefinery". This biorefinery concept has been proposed as a means to extract maximum value from lignocellulosic materials (forestry and agriculture biomass) for fuels, chemicals, and biomaterials production. One promising new product is cellulose nanocrystals (CNCs). Because of the biodegradability, the utility to increase surface properties in composites, and the unique properties extending to optical, liquid-crystalline, and self-assembly characteristics, CNCs have become one of the main focuses of research in the cellulosic field.[1,2] Meanwhile, because of their superior mechanical properties and large surface area, CNCs have also become more popular in several spheres of application, including packaging, drug delivery, cosmetics, photovoltaic devices, nanocomposites, etc.[3−6]

There are different types of nanocellulose forms, which will be briefly discussed at the beginning of this review along with their production and properties. However, the major concern in today's nanocellulose society is not about production but rather about finding a better application where its structural characteristics could be tailored by different methods. For the utilization and probably amplification of CNC properties, it is crucial to gain control over the molecular forces and physicochemical phenomena involved in its three-dimentional assembly processes.[7−10] There have been many approaches to assemble CNCs such as templating of chiral composites, layer-by-layer assemblies, host−guest functionalities, protein−hybrid composites, aerogels, and fiber spinning. However, most of these current assembly approaches could not take much advantage of the unique properties of CNCs. Lessons can be learned from nature, where a wide range of composite materials with outstanding mechanical, surficial, and optical properties (e.g., water lily leaves, butterfly wings, etc.) have been achieved with well-arranged structure at the nanoscale.[11−13]

Despite their great promise, to our knowledge there are no reviews to date that talk specifically about the alignment of cellulose nanocrystals and its applications. Hence, this review will highlight different current techniques to align CNCs such

Received: January 27, 2020
Accepted: March 23, 2020
Published: March 23, 2020

https://dx.doi.org/10.1021/acsabm.0c00104
ACS Appl. Bio Mater. 2020, 3, 1828−1844

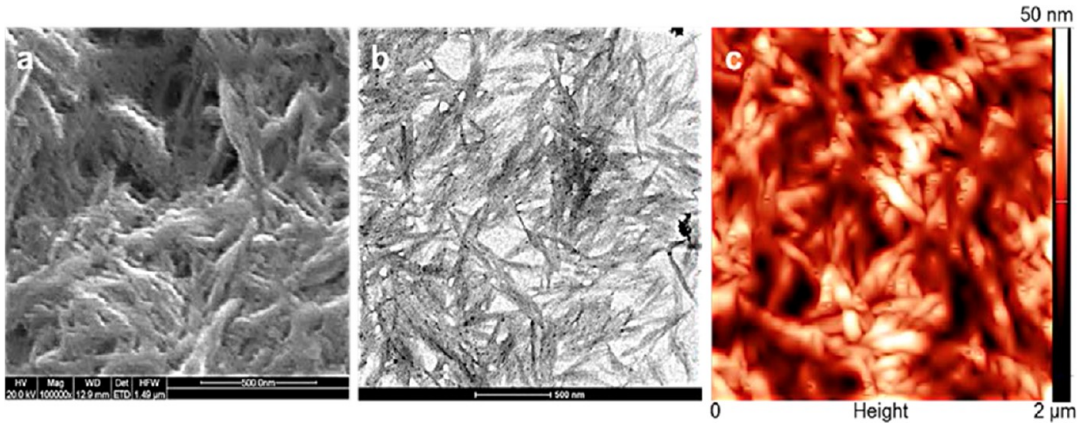

Figure 1. (a) Field-emission scanning electron microscopy (SEM), (b) transmission electron microscopy (TEM), and (c) atomic force microscopy (AFM) images of cellulose nanocrystals. Reproduced with permission from ref 41. Copyright 2013 Science and Education Publishing.

as self-assembly, shear-based alignment, magnetic and electric field alignment, spin-coating, dip-coating, etc. The later sections will then focus on highlighting the reported applications of such aligned cellulose nanocrystals, such as structural color for biomimetic applications; templates to align other nanomaterials and molecules; enhancement of the material strength of composites, aerogels, and films; tuning the surface properties of coatings (wettability, roughness, etc.); thin films for spectrometry; and biomedical and sensor applications. The different characterization techniques to quantify the CNC alignment will also be discussed. We hope that this review will shine light on CNC alignment and also open the door to different types of applications.

2. PREPARATION AND APPLICATIONS OF CELLULOSE NANOCRYSTALS

2.1. Preparation of Cellulose Nanocrystals. It is important to understand how CNCs are prepared from pristine cellulose through various physical and chemical treatments. A vast amount of information on structure, sources, and processing of cellulose has been reported extensively in the literature.[14−39] In the materials community, CNCs have garnered significant interest because of their abundance, inherent renewability, sustainability, and excellent physical and chemical properties.[19] Also, CNCs are promising candidates for reinforcing nanocomposites because of their low weight, low cost, nanoscale dimensions, and unique morphology. CNCs are also called different names in the literature, including nanocrystals, whiskers, and microcrystals.[40] Acid hydrolysis is the main process for isolation of CNCs from cellulose fibers. During acid hydrolysis (based on the acid concentration used), crystalline regions remain intact (as they are resistant to acid attack) whereas hydrolysis of disordered cellulose regions occurs.[19] Such an acid treatment produces rodlike cellulose nanocrystals. It was found that the morphology and crystallinity of the original cellulose fibers are retained in CNCs, as shown in Figure 1.[41] The kinetic difference in the hydrolysis rates for the crystalline and amorphous regions is the key factor for controlled acid cleavage, and hence, crystalline regions remain while amorphous regions are hydrolyzed readily.

The preparation of CNCs is affected by parameters such as the acid-to-cellulosic fiber ratio and the nature and concentration of the acid used. Purification of suspensions after acid treatment involves repeated centrifugations and dialysis for several days. For the acid hydrolysis treatment of CNCs, sulfuric or hydrochloric acid is commonly used. Nevertheless, acid cleavage using phosphoric[42,43] or hydrobromic acid[44] has also been reported. It was found that CNCs flocculated and their ability to disperse was limited if the hydrolysis was undertaken using hydrochloric acid.[45] However, with sulfuric acid hydrolysis, better dispersion of CNCs in water was observed because of the production of charged surface sulfate esters by the reaction of the acid with the surface hydroxyl groups of cellulose. The downside of this approach is that the thermal stability of the nanocrystals is compromised with the introduction of charged sulfate groups.[46] Another reason that hydrochloric acid is less attractive for hydrolysis is apparent from rheological behavior differences. It was seen that a suspension treated with hydrochloric acid showed thixotropic and antithixotropic behavior at concentrations of 0.5% and 0.3% respectively,[45] whereas with sulfuric acid no time-dependent viscosity of the suspension was observed. It was seen that spherical CNCs were obtained when the hydrolysis was carried out using a combination of hydrochloric and sulfuric acids with concurrent ultrasonic treatment.[47,48] As these spherical CNCs possess fewer sulfate groups on their surfaces, they exhibit good thermal stability.[48] Bondeson et al. demonstrated that a CNC yield of 30% with lengths between 200 and 400 nm and widths less than 10 nm could be obtained by the use of sulfuric acid at a concentration of 63.5% (w/w) over 2 h.[49,50]

A decrease in nanocrystal length and increased surface charge were observed when the hydrolysis time was prolonged for several hours.[51] On the basis of the hydrolysis conditions and cellulosic material source, the geometry of CNCs can vary widely because the acid hydrolysis is diffusion-controlled. Chemical functionalization of CNCs is carried out either by introducing positively or negatively charged groups on their surfaces or by tuning their surface energy characteristics, improving their dispersion and compatibility in composites. Lu and Hsieh used cotton cellulose as the starting material for cellulose nanocrystal preparation, wherein acid hydrolysis followed by freeze-drying yielded rodlike, spherical, and network morphologies, as shown in Figure 2.[52] Dispersion in aqueous media was facilitated by the sulfate groups introduced by sulfuric acid hydrolysis, whereas improved specific surface area and mesoporosity were induced by freeze-drying.

Few works have been reported with respect to preparation of cellulose nanocrystals using physical treatments. Li et al. used

https://dx.doi.org/10.1021/acsabm.0c00104
ACS Appl. Bio Mater. 2020, 3, 1828−1844

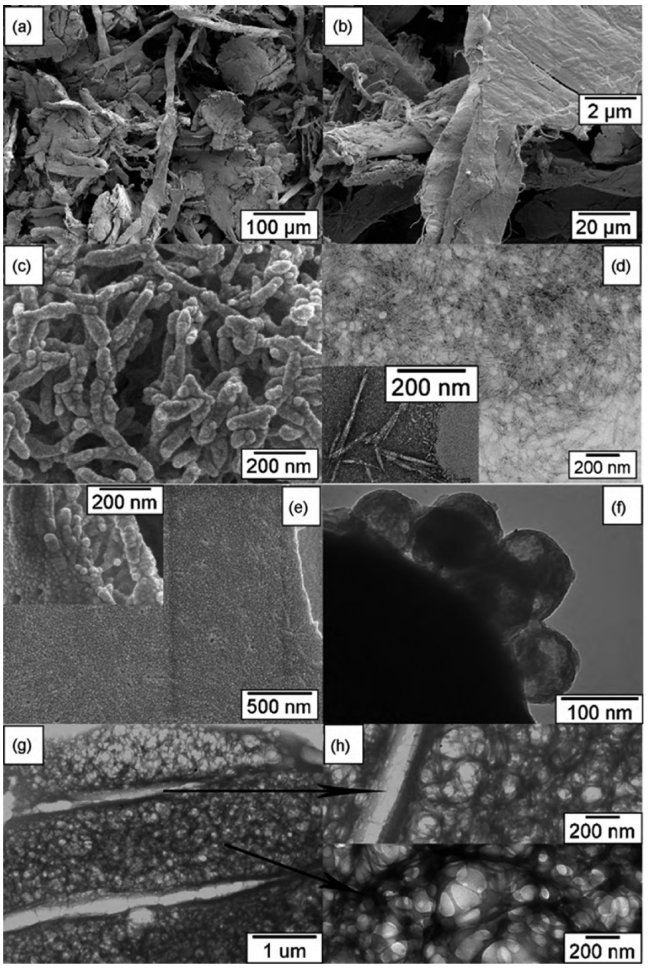

Figure 2. SEM images of (a, b) cellulose powder, (c) rod-shaped CNCs, and (e) spherical-shaped CNCs and TEM images to study the (d) rod-shaped, (f) spherical-shaped, and (g, h) porous-network-shaped cellulose nanocrystals prepared. Reproduced with permission from ref 52. Copyright 2010 Elsevier Ltd.

high-intensity ultrasonication to prepare rod-shaped CNCs (diameter: 10−20 nm; length: 50−250 nm) from microcrystalline cellulose (MCC).[53] Ultrasonication treatment had an inverse effect on the crystallinity and length of the CNCs prepared. Nevertheless, the technique is limited by its nonselective nature, cleaving both crystalline and amorphous parts of MCC (Figure 3). An ultrasonically assisted enzymatic process was used to prepare CNCs from wheat MCC.[54] The resulting nanocrystals had widths of less than 10 nm and lengths of 40−50 nm, which were sensitive to the ultrasonication process. Tang et al. observed the morphological similarity of cellulose nanocrystals prepared via acid hydrolysis with and without ultrasonic treatment;[55] the yield was slightly higher when ultrasonic treatment was used. A similar study was also carried out by Guo et al. to explore the effects of ultrasonication treatments on the CNC structure.[56] A disordered CNC structure was obtained when the CNCs were subjected to prolonged acid attack under ultrasonication. Similar effects were also observed in the work reported by Li et al., wherein surface erosion and cellulose folding of the bleached softwood kraft pulp along with reduced CNC length occurred during ultrasonication for the preparation of CNCs.[57] A $FeCl_3$-catalyzed hydrolysis technique assisted by ultrasonication was used to prepare CNCs from bamboo pulp.[58] The prepared CNCs had a rod-shaped morphology and formed an interconnected network structure with a width of 10−20 nm and length of 100−200 nm. The conventional acid-based hydrolysis technique was found to yield cellulose nanocrystals of poor thermal stability, and the use of strong acids and solvents makes it industrially laborious.[48] Hydrothermal treatment using hydrochloric acid and treatments with a mild acid such as phosphoric acid have also been used to prepare thermally stable CNCs.[59,60] However, the prepared CNCs showed poor scalability and low yield. Recently, high-energy bead milling (Figure 4) was employed to isolate rod-shaped CNCs (freeze-dried) from MCC in an aqueous medium.[61] The obtained yields were between 57 and 76%, and the CNCs were found to be thermally stable (degradation temperature: 250 °C). Irrespective of the high yield, the technique may not be viable for industrial purposes because of the contamination of cellulose nanocrystals with zirconium (in high ppm quantities) and the aggregation of cellulose nanocrystals due to the effects of the high energy imparted during the ball milling technique.

2.2. Applications of Cellulose Nanocrystals. Because of their intrinsic properties such as high surface area and mechanical strength, CNCs find immense applications in the nanocomposites field.[62] The presence of hydroxyl functional groups makes them readily available for chemical functionalization, facilitating their incorporation into various polymer matrices.[63−67] These polymer composites find applications in packaging, textiles, coatings, and automobile parts. To detect the in vivo interaction of cellulose nanocrystals with cells, cellulose nanocrystals have been fluorescently labeled using a three-step reaction pathway (Figure 5).[68] The process dissolves softwood pulp using sulfuric acid and incorporates covalently bonded fluorescent molecules onto cellulose nanocrystal surface to enable fluorescent detection of the CNC location in vivo.

The thermal and mechanical performance of polyurethane-based composites was found to be affected by the addition of cellulose nanocrystals during polymerization. The addition of cellulose nanocrystals acted as the limiting factor for the deformation and modulus of the nanocomposites synthesized.[69] A decrease in thermal resistance was found when cellulose whiskers were incorporated as a filler into poly(lactic acid) (PLA) nanocomposites.[70] Depending on the concentration of the filler, the mechanical properties (modulus) of the composite varied by enhancement of the brittleness of the PLA nanocomposites.[71] A decrease in tensile storage modulus was observed when a percolated network of cellulose whiskers was introduced into poly(vinyl acetate) under simulated physiological conditions.[72] The materials prepared also exhibited decreased swelling, which could potentially be used for other biomedical applications.[72] Composite sheets were prepared using a solution-casting method to incorporate cellulose nanocrystals into poly(methyl methacrylate) nanocomposites, retaining the material's transparency. The introduction of CNCs enhanced the storage modulus and thermal stability of the prepared nanocomposite.[73] Cellulose nanowhiskers assembled layer by layer with chitosan were used to prepare a biodegradable nanocomposite with high density. The prepared nanocomposite used nanowhiskers obtained from eucalyptus wood pulp by acid hydrolysis, which were homogeneously distributed within the chitosan layers, and served as a high-performance renewable material.[74] The methodology used in preparation of these nanocomposites

https://dx.doi.org/10.1021/acsabm.0c00104
ACS Appl. Bio Mater. 2020, 3, 1828−1844

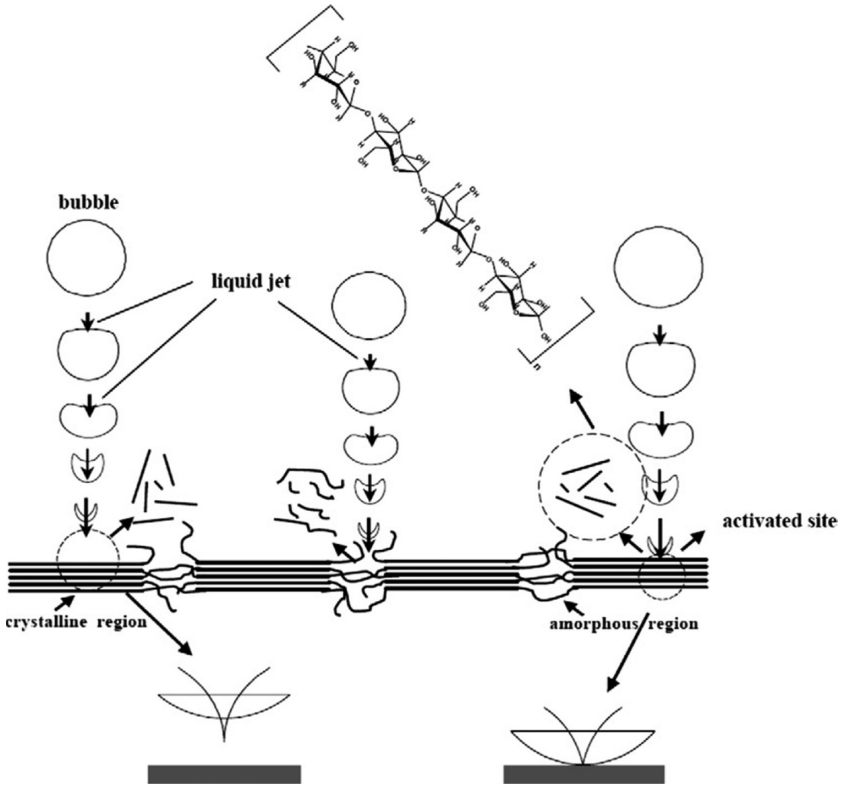

Figure 3. Schematic diagram illustrating ultrasonication treatment to produce cellulose nanocrystals from microcrystalline cellulose. Reproduced with permission from ref 53. Crown copyright 2011, published by Elsevier B.V.

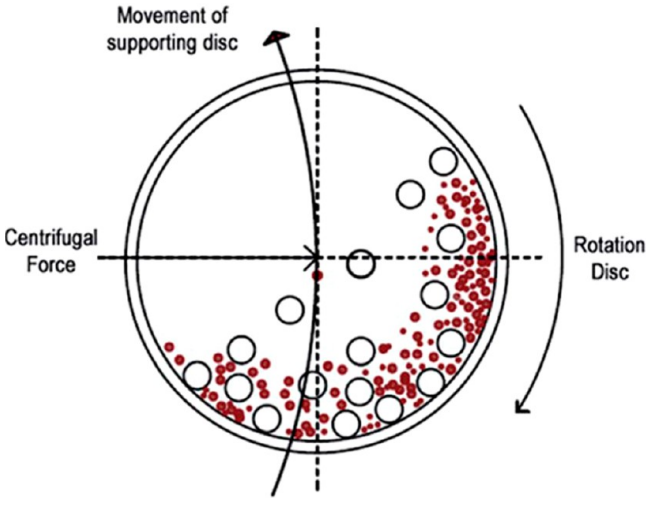

Figure 4. Schematic diagram illustrating the high-energy bead milling technique for producing thermally stable cellulose nanocrystals. Reproduced with permission from ref 61. Copyright 2015 Royal Society of Chemistry.

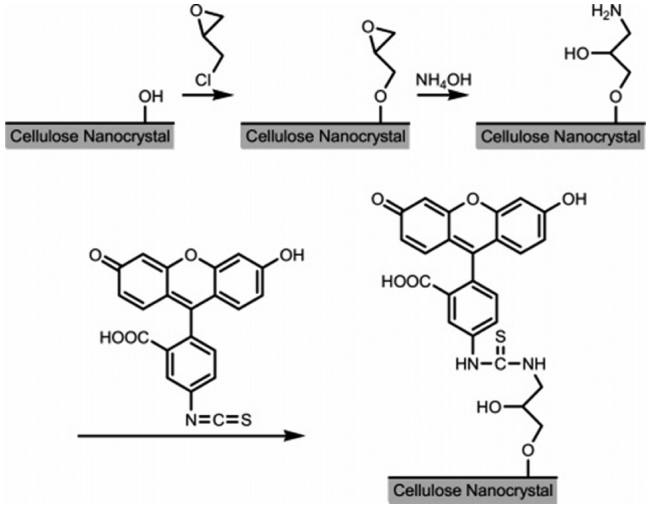

Figure 5. Schematic diagram illustrating the three-step pathway by which cellulose nanocrystals are fluorescently labeled. Reproduced from ref 68. Copyright 2007 American Chemical Society.

could be extended to the preparation of new bio-based nanocomposites that could be used in several applications, including food packaging and biomedical applications. Recently, cellulose nanocrystals were used in coating technologies for drug delivery applications because of their nontoxic behavior.[75−77]

Cationic functionalization of cellulose nanocrystals was carried out by Hasani et al. using epoxypropyl trimethylammonium chloride (EPTMAC).[78] The functionalized cellulose nanocrystals (Figure 6) were obtained from cotton via acid hydrolysis and showed reduced total surface charge density, resulting in unexpected rheological and gelling properties and the ability to form stable aqueous suspensions.[78] Similar surface modification of cellulose nanocrystals was carried out by Salajkova et al. using quaternary ammonium salts.[79] Strong birefringence was observed for modified CNCs suspended in toluene, and a water contact angle increase from 12° to 71° was found upon modification of the CNCs. Various other surface-functionalized CNCs have been reported to form stable CNC suspensions with either enhanced hydrophobicity or birefringence.[80−82] Eyley and Thielemans reported different

https://dx.doi.org/10.1021/acsabm.0c00104
ACS Appl. Bio Mater. 2020, 3, 1828−1844

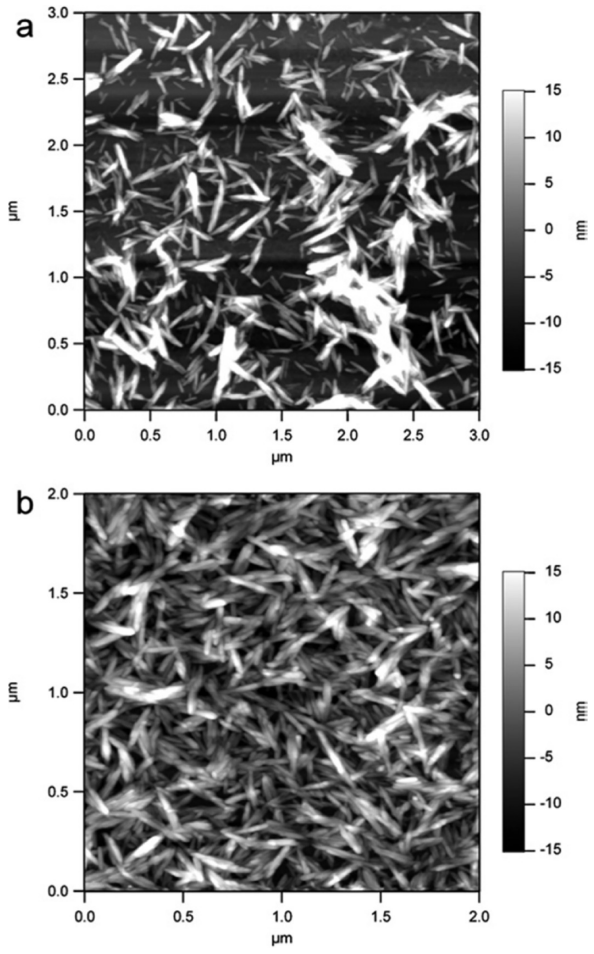

Figure 6. AFM images of cellulose nanocrystals prepared via acid hydrolysis of cotton as the source material (a) without and (b) with surface functionalization with EPTMAC. Reproduced with permission from ref 78. Copyright 2008 Royal Society of Chemistry.

methods for surface modification of cellulose nanocrystals, including oxidation, esterification, amidation, carbamation, etherification, and nucleophilic substitution.[83] However, in this review, less emphasis is placed on such chemical modifications, which affect the surface functional groups and change the surface characteristics.

3. ALIGNMENT OF CELLULOSE NANOCRYSTALS

3.1. Self-Assembly of Cellulose Nanocrystals. Negatively charged sulfate groups are created on the surface of CNCs upon acid hydrolysis of microfibrillated cellulose (MFC) using sulfuric acid, and these groups electrostatically repel each other, resulting in the formation of stable CNC dispersions. To minimize these electrostatic interactions, cellulose nanocrystals in concentrated suspensions configure themselves to give specific local orientations.[19] Similar self-assembly was seen with other rodlike structures that exist as nonflocculating suspensions.[84−86] Chiral nematic liquid-crystalline structure, characterized by a fingerprint-like pattern, occurs as a result of this self-assembly, which could be observed using an optical microscope in crossed-polarization mode.[87] Such an ordered chiral nematic phase (Figure 7) occurs only when the concentration of CNCs reaches a critical concentration, forming an orientationally anisotropic phase.[88,89] Shear birefringence is shown by the CNCs at

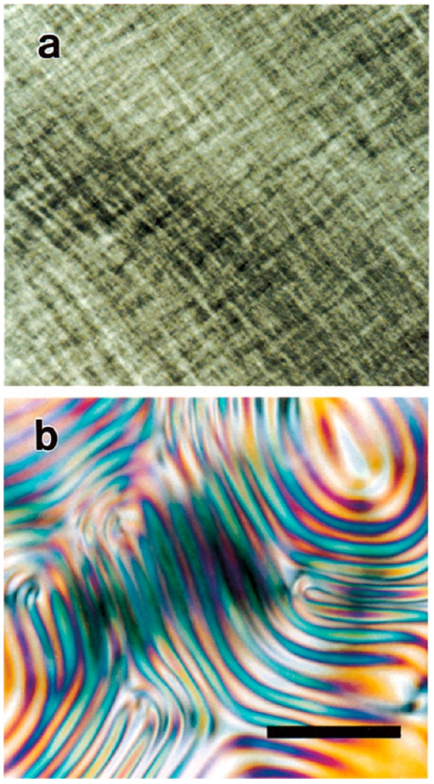

Figure 7. Polarized optical microscopy images of cellulose nanocrystal suspensions showing (a) a 7.1% post-sulfated suspension with cross hatch pattern and (b) a chiral nematic structure with 5.4% solid content exhibiting a fingerprint structure obtained during acid hydrolysis. Scale bar: 200 μm. Reproduced from ref 89. Copyright 2000 American Chemical Society.

concentrations above the critical concentration.[90] Certain studies have revealed that such chiral nematic order may be attributed to a twist in CNCs, which is inherent in the cellulose backbone and the crystalline material.[87,91] More evidence of such twisting was also provided by studies carried out on surfactant-stabilized CNC suspensions.[92] These chiral nematic structures go on to form iridescent films upon complete water evaporation. Numerous applications utilize such solid films, including security papers and optical coating materials.[93−95] The chiral nematic phase self-assembly of cellulose nanocrystal suspensions was studied by Roman and Gray.[96] Slow evaporation of the suspension resulted in the formation of parabolic focal conic (PFC) defects, which were characterized using atomic force microscopy and polarized light. The ordering of cellulose nanocrystals at concentrations below this chiral nematic phase transition is however a challenge. As will be elaborated more below, many approaches to align CNCs have been attempted, such as using magnetic alignment, electric field alignment, shear-based alignment, etc., but most of the time these techniques exhibit only local alignment and also possess limitations with respect to processing parameters and scalability.

3.2. Shear-Based Alignment of Cellulose Nanocrystals. Alignment of CNCs in the direction of a shear flow was observed by Orts et al. using small-angle neutron scattering (SANS), wherein the neutron beam was passed perpendicular to the shear flow.[97] An increase in alignment of CNCs with shear rates from 0.1 to 7000 s^{-1} was clearly observed. A similar study was carried out by Ebeling et al. in which two shear rates

https://dx.doi.org/10.1021/acsabm.0c00104
ACS Appl. Bio Mater. 2020, 3, 1828−1844

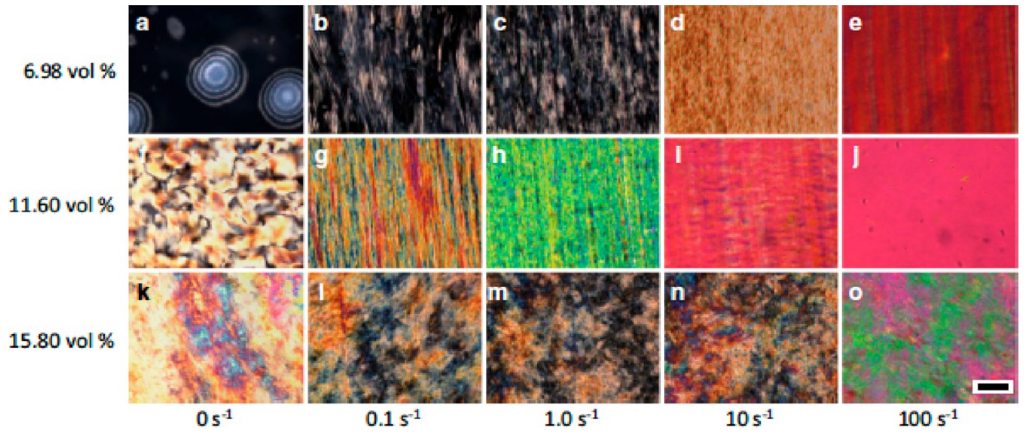

Figure 8. CNC dispersions at different concentrations subjected to varying shear rates (flow direction upward), observed using optical microscopy in cross-polarization mode. (a–o) Scale bar: 100 μm. Reproduced with permission from ref 100. Copyright 2016 Springer Science Business Media Dordrecht.

were used to align CNCs perpendicular to and parallel to the shear direction at low (5 s^{-1}) and high (500 s^{-1}) shear rates, respectively.[98] The study indicated that the orientation of CNCs could be controlled by adjusting the shear rate. The order parameter for isotropic and anisotropic CNC configurations prepared using various shear rates was studied by Chowdhury et al.[99] The study was carried out to investigate the crystal orientation using UV–vis spectrophotometry, a low-cost and simple technique. Various shear rates were used to prepare self-standing CNC films with short-range order. Order parameters were calculated by determining the dichroitic ratio, which was evaluated from the transmitted light intensity of the CNC films when they were placed between crossed polarizers. Compared with other traditional techniques, the birefringent method employed was inexpensive and reproducible. Details about characterizing the aligned CNCs to evaluate the order parameter will be discussed in later sections.

Optical contrast measurements (Figure 8) were used by Haywood and Davis to study the microstructural relaxation effects of shear forces on alignment of CNC films.[100] The final structure of CNC films was primarily affected by the combined effects of rheology, relaxation, and dispersion microstructure in the initial stage. Doctor blade coating has been used to shear align CNCs. After relaxation, CNCs coated from an isotropic phase did not align at lower concentrations. However, at higher concentrations, the degree of freedom[101] decreased, as a result of which CNCs aligned at shear rates up to 100 s^{-1}. The alignment of CNCs in liquid-crystalline dispersions using shear rates from 25 to 100 s^{-1} was found to be comparatively easier because of the self-assembly of CNCs in the nematic phase.[102]

Uniformly oriented cholesteric CNC helices were prepared by Park et al. using a circular-shear-based method whereby vertical helix orientation was achieved when the concentration of CNCs used was increased into the liquid-crystalline range.[103] Shear-induced alignment of CNCs using an in-line polarized light imaging integrated single-droplet oscillatory system (a complex microfluidic imaging technique) was studied by Alizadehgiashi et al.[104] The alignment of CNCs was analyzed using an oscillating droplet of isotropic aqueous CNC suspension (in a capillary) and was found to be affected by the suspension viscosity and the shear rate. Alignment of CNCs in fibers using shear-based forces produced by hydrodynamic flow and spinning has also been reported in the literature.[105,106] Grazing-incidence wide-angle X-ray scattering (GIWAXS) was used by Sanchez-Botero et al. to measure aligned CNCs at different concentrations (7 and 9 wt %) and to study the influence of other process parameters such as shear-cast velocity and solution concentration on the CNC ordering.[107] X-rays were focused onto a cast film made from CNCs, and GIWAXS patterns were recorded at fixed intervals of time. It was found that the process parameters (shear velocity, evaporation rate, and concentration of the precursor suspension) had a negligible influence on the CNC orientation.

Convective and shear-based forces were used by Hoeger et al. to align CNCs deposited as ultrathin films on solid supports.[108] Image analysis was used to measure the degree of CNC orientation. A CNC concentration of 2.5% w/w, far lower than the critical concentration for chiral nematic phase formation, was used for alignment, wherein the CNCs aligned well in the shear withdrawal direction supported by gold and silica substrates. The mechanical strength and wear resistance of the prepared ultrathin film was enhanced by the shear-based alignment.

3.3. Magnetic Alignment of Cellulose Nanocrystals. A magnetic field of 1.2 T was used by Pullawan et al. to align cellulose nanowhiskers (derived from tunicates) that were incorporated into a cellulose matrix system.[109] The volume fraction of cellulose nanowhiskers was found to be a key criterion affecting the mechanical properties of the final composite material. It was found that lowering the volume fraction of these cellulose nanowhiskers makes them readily orient under the applied magnetic field. The oriented cellulose nanowhiskers were found to impart enhanced strength and stiffness to the composite. However, the orientation under a 1.2 T magnetic field was incomplete, as 50% of the cellulose nanowhiskers remained misaligned with the magnetic field. A similar study on aligning cellulose nanowhiskers using a magnetic field (1.2 T) was carried out by Li et al. in order to fabricate reinforced nanocomposite paper.[110] The paper was made by aligning the nanowhiskers in wood pulp under the influence of magnetic fields, wherein the negative diamagnetic anisotropy of the nanowhiskers was found to be the key characteristic for magnetic alignment. The fabricated nanocomposite paper was found to have a stronger storage modulus in the direction perpendicular to the applied magnetic field but was weak in the direction parallel to the magnetic field (Figure

https://dx.doi.org/10.1021/acsabm.0c00104
ACS Appl. Bio Mater. 2020, 3, 1828–1844

9). However, only local alignment of cellulose nanowhiskers under the applied magnetic field was again seen.

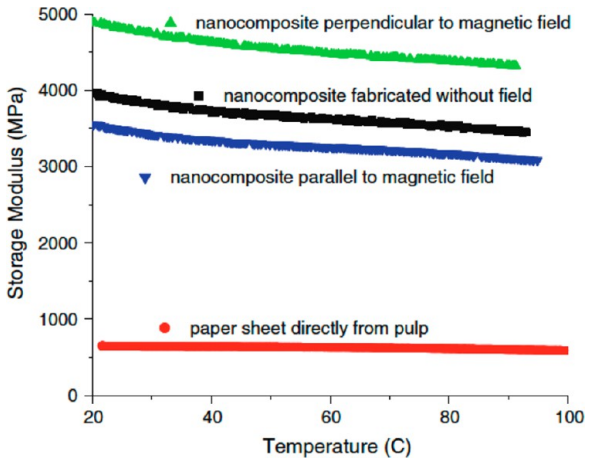

Figure 9. Comparison of storage moduli of cellulose-nanowhisker-reinforced nanocomposites in the presence and absence of a magnetic field. Reproduced with permission from ref 110. Copyright 2010 Springer-Verlag.

A noninvasive approach for aligning CNCs using Fe_3O_4 (51 wt %) in a low magnetic field (~60 mT) was reported by Dhar et al.[111] In situ precipitation was used to facilitate the adsorption of Fe_3O_4 nanoparticles onto the CNCs. PLA was used to disperse these nanofillers, in which the CNCs were aligned in the magnetic field (because of the high magnetic moment of the iron oxide nanoparticles). The resultant nanocomposite film was found to possess improved electrical and thermal properties compared with the nonaligned nanocomposite.[111] However, the loading of iron oxide nanoparticles required was very high, limiting its practical application.

Sugiyama et al. were the first to report the magnetic alignment of cellulose microcrystals under a strong magnetic field (7 T).[112] Because of the diamagnetic susceptibility response of cellulose, the fiber axis of the microcrystals was oriented perpendicular to the direction of the magnetic field. Two different types of magnetic field, static and rotating, were used by Kimura et al. to align tunicate cellulose microfibrils at a concentration above the critical transition concentration, in which the effect of the static magnetic field was to align the small chiral nematic domains into a monodomain and the rotating magnetic field was used to drive the chiral nematic phase into the nematic phase.[113] The microfibrils were prepared from cellulosic mantles of tunicin using acid hydrolysis. The direction perpendicular to the fiber axis showed higher diamagnetic susceptibility compared with the direction parallel to the fiber axis. The reported work may not be feasible for industrial purposes, however, as very high magnetic fields ranging from 5 to 28 T were used to achieve alignment. Similar work on alignment of cellulose nanofibers (prepared from regenerated cellulose) under the influence of a strong magnetic field (7 T) was reported by Kim et al.[114] The decomposition temperature of the material was found to be higher when the nanofibers were aligned using a strong magnetic field.

Revol et al. reported the magnetic alignment (7 T) of cellulose nanocrystals (axial ratio: 20−40) in the chiral nematic liquid-crystalline phase.[115] The chiral nematic axis, owing to the negative diamagnetic susceptibility, is oriented parallel to the applied magnetic field. Iridescent cellulose nanocrystal films were prepared by Edgar and Gray from cellulose suspensions under the influence of a magnetic field of 7 T produced within an NMR spectrometer.[116] The chiral nematic order of the prepared film was found to increase with the applied magnetic field, which was recorded by measuring induced circular dichroism changes.

Kvien and Oksman used a strong magnetic field of 7 T to align nanowhiskers in a poly(vinyl alcohol) matrix.[117] Enhancement of the dynamic modulus of the nanocomposite by a value of 2 GPa was found in the direction of aligned cellulose nanowhiskers compared with the perpendicular direction. A composite of cationic polymer with cellulose nanocrystals in the chiral nematic phase was used by Cranston and Gray to form a polyelectrolyte film via layer-by-layer assembly.[118] The cellulose nanocrystals in the polyelectrolyte film were oriented in a magnetic field of 7 T. Even though the orientation of the nanocrystals was successful, long (~24 h) exposure to the magnetic field was required to achieve complete alignment.

Even though many works have reported magnetic field alignment of cellulose nanocrystals, most of them used high magnetic field strengths (above 5 T), which are not suitable for scalable processing. The low magnetic field alignment of cellulose nanocrystals reported showed only local alignment.

3.4. Electric Field Alignment of Cellulose Nanocrystals. The alignment of rod-shaped particles[119,120] was previously studied using electric fields, wherein electric birefringence[121] was found to be the main reason for orientation of these particles under the influence of the electric field. The electric field alignment of cellulose nanocrystals was initially studied by Bordel et al. at frequencies ranging from 10 Hz to 10 kHz, wherein nonpolar solvents were used to suspend the CNCs to avoid issues arising from the high conductivity of water.[122] When an electric field of strength of 1200 V/cm was applied, the long axis of the CNCs was oriented parallel to the direction of the applied electric field. Habibi et al. used electric field alignment (2000 V/cm; frequency: 10^4−10^6 Hz) to orient a cellulose nanocrystal suspension.[123] It was found that the strength and frequency of the applied electric field greatly influenced the orientation of cellulose nanocrystals (Figure 10).

A coupled mechanism of dielectrophoresis along with convective shear-based assembly was used by Csoka et al. to align CNCs.[124] The dielectrophoresis used a low electric field strength of 400 V/cm at a frequency of ~2000 Hz. A shear rate of 8.4 cm/h was applied to 2.5 wt % CNC suspensions dispersed between mica substrates under the influence of an electric field that oriented the CNCs. The coupled mechanism resulted in greater alignment of CNCs compared with the alignment using either technique separately.[124] Alignment of CNCs using apolar solvents under the influence of DC and AC electric field systems were studied by Frka-Petesic et al.[125] Nevertheless, the two configuration systems (DC and AC) resulted in a similar order of magnitude of the electric dipole moments (permanent and induced dipoles under the influence of electric field) of CNCs. Even though alignment of CNCs was demonstrated using an electric field,[122] the use of toxic solvents renders this method industrially undesirable.

3.5. Other Techniques for Aligning Cellulose Nanocrystals. Many other techniques for aligning cellulose nanocrystals have been reported in the literature, including

https://dx.doi.org/10.1021/acsabm.0c00104
ACS Appl. Bio Mater. 2020, 3, 1828−1844

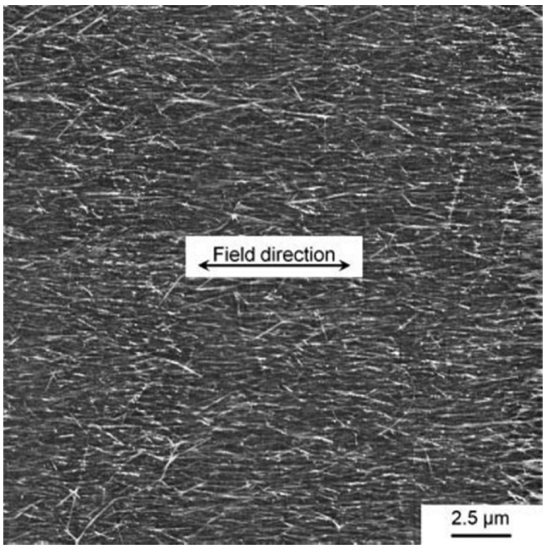

Figure 10. AFM image showing the alignment of CNC films (tunicate source) under the influence of an electric field with a strength of 10 V and a frequency of 250 kHz. Reproduced with permission from ref 123. Copyright 2008 John Wiley and Sons.

spin-coating, dip-coating, electrospinning, freeze-drying, etc.[126−132] Nevertheless, these techniques again fail in achieving the desired global alignment. High levels of alignment of cellulose nanocrystals were achieved by unidirectional freezing of nanocellulose dispersions:[126] CNCs at 0.2 wt % aligned in the freezing direction. A stronger resistance to melting was observed from the directionally frozen nanocellulose network.[126] Huan et al. fabricated reinforced PLA fiber mats using electrospinning, wherein 20 wt % CNCs were incorporated into the polymer matrix for electrospinning.[127] The alignment technique was found to influence the porous structure of the final composite and also resulted in the production of fiber mats with a high degree of crystallinity compared with mats made using random CNCs. Also, enhancement of the thermal and mechanical properties of the PLA composite was found with the aligned fibrous structure.[127] A similar use of cellulose nanocrystals for reinforcement was reported by Song et al., wherein electrospinning was used to create aligned poly(vinyl acetate) (PVA)/cellulose nanocrystal composites.[128] High tensile strength was observed for the aligned nanofibrous composite, along with continuous birefringence, due to the nematic phase of CNC.

Thin films of CNCs exhibiting iridescent color due to thin-film interference (based on film thickness and refractive index) were prepared by spin-coating CNCs onto reflective substrates.[129] The spin-coating conditions, including spin speed (rpm), duration of spinning, and concentration of CNC suspension used, are the main factors governing the ordering of CNCs using spin-coating.[130] Aligned CNC templates prepared using spin-coating were used to orient muscle cells (myoblasts) that aligned in the direction of the aligned CNCs.[131] The aligned CNCs for this purpose were fabricated by spin-coating CNCs (tunicate-derived) onto a glass slide coated with a cationic polyelectrolyte. Very poor orientation of CNCs was observed for multilayer films of CNCs with a cationic polyelectrolyte fabricated using a combination of spin-coating and dip-coating techniques.[132] Aligned CNC films using dip-coating have been reported in the literature, wherein the orientation parameter was controlled by the dipping shear action and dipping time.[133] Nevertheless, this technique is not feasible for large-scale production because of the weak degree of orientation obtained. Stable oriented CNC layers were prepared using Langmuir−Schaeffer (LS) and Langmuir−Blodgett (LB) methods with the help of a cationic surfactant.[134,135] Nonradial and uniaxial alignment of CNCs was achieved using LB and LS techniques. The surfactant after film deposition was removed using chloroform.[135] The alignment of CNCs using the LS technique was mainly attributed to the self-assembly of CNCs resulting in nematic configurations.[134] However, as discussed earlier, none of the reported techniques was successful in achieving perfect orientation globally.

A new fascinating technology known as wrinkling technology was recently reported in which wrinkles were created on poly(dimethylsiloxane) (PDMS) substrates upon relaxation of stretched PDMS after plasma exposure.[136,137] The key factors for wrinkle production were the plasma exposure time, plasma power, strain conditions, and the type of substrates used.[137] To date in the field of alignment of cellulose nanocrystals, very few studies have been reported with respect to alignment using wrinkling technology. Nystrom et al. used different wrinkle periodicities to align rod-shaped cellulose nanocrystals that were transferred to a poly(ethylenimine) (PEI)-treated silica surface using 1 μL of Milli-Q water in a so-called water-mediated transfer process (Figure 11).[138] The transferred CNCs were aligned perfectly, showing global alignment order. However, the study raises questions regarding the efficient transfer of CNC particles to the intended substrate and also the robustness of using PEI-coated substrates for CNC

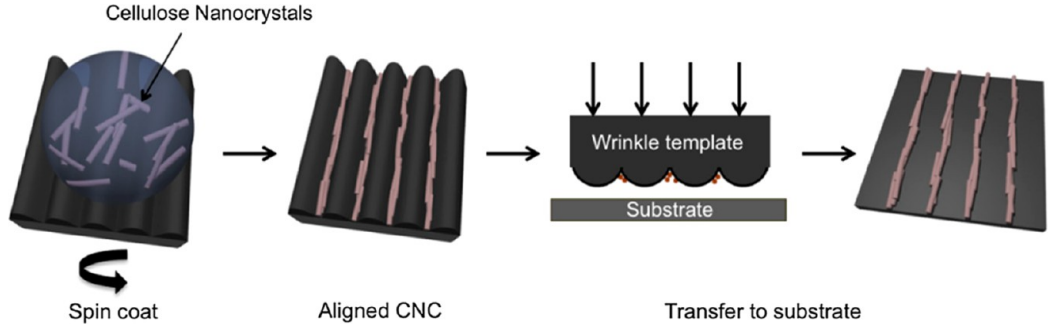

Figure 11. Schematic diagram showing the use of wrinkling technology to align cellulose nanocrystals using a water-mediated transfer process. Reproduced with permission from ref 138. Copyright 2014 Springer Science Business Media Dordrecht.

https://dx.doi.org/10.1021/acsabm.0c00104
ACS Appl. Bio Mater. 2020, 3, 1828−1844

alignment. A similar procedure for aligning CNCs was carried out by Prathapan et al. to evaluate the wetting behavior of water droplets on a cationic polyelectrolyte/aligned CNC-coated glass surface.[139] It was found that the contact angle remarkably increased with surface structuring because of pinning effects and higher contact angle hysteresis, thereby facilitating an alternative constructive approach to surface chemical functionalization of CNCs to achieve hydrophobic surfaces (Figure 12).

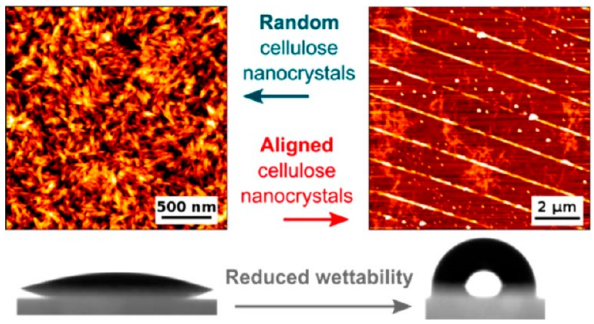

Figure 12. Schematic diagram depicting the increase in contact angle on aligned cellulose nanocrystal coatings fabricated by wrinkling method. Reproduced from ref 139. Copyright 2017 American Chemical Society.

4. CHARACTERIZATION OF ALIGNED CELLULOSE NANOCRYSTALS

Once alignment of CNCs is achieved, it is very important to confirm the alignment through various characterization techniques, including morphological analysis, X-ray diffraction (XRD) patterns, birefringence studies, and other spectroscopic studies. The main focus of these techniques relies on calculation of the alignment parameters that define the alignment in a quantitative manner. Here, the current main techniques to quantify and qualify the CNC alignment are briefly reviewed to provide guidance for readers who would like to explore this research direction.

Morphological characterization of aligned CNCs can be achieved using imaging techniques like scanning electron microscopy (SEM) and atomic force microscopy (AFM). Even though other morphological characterizations like transmission electron microscopy (TEM) and confocal microscopy could be used to analyze the alignment, AFM and SEM have been commonly utilized since the acquired images can be easily processed to further quantify the CNC alignment using various available imaging software packages. Fundamentally, SEM records images based on the scattering of electrons incident on the sample surface,[140] while AFM on the other hand analyzes the cantilever deflection based on the surface topography.[141] Therefore, parameters for quantifying the alignment could be calculated from these derived images. For example, using OrientationJ,[142] the degree of ordering can be quantified from the SEM images, wherein the gray level in a local neighborhood of SEM images can be used to analyze the degree of ordering. During this process, the angle of predominant orientation, α_{max}, is defined using the maximum of the Gaussian distribution of the orientation angle α, which corroborates the wrinkle direction.[143] The degree of ordering is then quantified by analyzing the deviation from this predominant direction. On the other hand, periodic structures with atomic accuracy could be characterized using Fourier Transforms, a software that can be utilized once the image scanning is completed in an AFM experiment.[144] For characterizing structure periodicity and surface anisotropy, Arutyunov et al. has formulated an analytical method by which space parameters like the texture direction index and texture direction can be calculated from the Fourier transforms.[145] To define the surface topography of materials, power spectral density (PSD) functions can be used.[146,147] The distribution of surface height with wavenumber can be detailed using PSD, which uses the frequency domain of AFM images with the help of Fourier transform theory.[148] Thus, from the wavelengths recorded in the surface spectrum, the orientation and periodicity of surface features can be characterized.[149]

For analysis of aligned materials or periodic structures, the wide-angle X-ray diffraction (WAXD) technique is widely employed.[150−155] The image scanning is carried out both parallel and perpendicular to the sample surface, so as to effectively analyze the effect of aligned features. The azimuthal intensity profiles of the crystallographic lattice planes (especially the 200 plane) are obtained from WAXD images and used to quantify the degree of alignment of sample structures.[156] The orientation index π and orientation parameter s reflect the degree of sample alignment: $\pi/s = 1$ corresponds to a perfectly aligned surface, whereas $\pi/s = 0$ refers to randomly oriented sample features.[157] The details of the calculation of π and s have been reported by Yao et al.[158] The same concept of calculating orientation parameters has also been used in small-angle X-ray scattering (SAXS).[159] However, for crystalline periodic structures, WAXD is more appropriate and consistent.

Calculation of the orientation distribution based on refractive index differences and optical anisotropy can be achieved using birefringence studies. For determination of the refractive index, ellipsometry is commonly used, but its analysis is limited to only low surface roughness.[160] Chowdhury et al. developed novel UV−vis spectroscopy-based optical measurements for studying the birefringence of CNC materials.[99] The order parameter (Herman's order parameter) for the sample surface is calculated using the dichotic ratio, a comparison of the bright- and dark-field intensities of the sample surface.[161] The alignment order parameter calculation involves sample characterization using the UV−vis spectrophotometer, wherein the sample surface is kept between linear crossed polarizers. Transmittance data are then collected with maximum intensity in the bright field and dark field at 45° and 90° positions with respect to the sample and the adjacent polarizers. Distinct differences in the peak intensities at the 90° and 45° configurations can be observed for aligned CNC films. The maximum light intensity is observed for the aligned CNC surface at 45°, whereas the total transmission from the 90°-configured aligned CNC surface is a minimum.[99]

Other methods, including Raman spectroscopy,[162] polarized infrared spectroscopy,[163] and polarized fluorescence microscopy,[164] could be also utilized in determining the orientation parameters in semicrystalline polymers. However, such methods are not so frequently used because of the difficulty in interpreting data to calculate the order parameter values.[99]

5. APPLICATIONS OF ALIGNED CELLULOSE NANOCRYSTALS

In the above sections, we have discussed the different ways of aligning CNCs and characterizing the alignment. This section

https://dx.doi.org/10.1021/acsabm.0c00104
ACS Appl. Bio Mater. 2020, 3, 1828−1844

will highlight the major current applications of these aligned CNCs and also discuss their potential further applications. To date, the main applications of aligned CNCs include enhancing material strength, surface properties, structural color, and biomedical applications.

A sustainable bioinspired nanocomposite based on aligned CNCs with enhanced mechanical properties was demonstrated by Wang et al.,[165] where CNCs were aligned in a matrix of carboxymethylcellulose using an effective drawing procedure and significantly improved the strength of the assembled nanocomposite. Cellular structures with tailored mechanical properties could be achieved using anisotropic CNCs that are shear-aligned using the 3D printing technique.[166] Since the ink for 3D printing is aqueous in nature, introducing hydrophilic CNCs yields enhanced stiffness for the textured composites along the printing direction. Shear-aligned cellulose nanocrystal films were also used to fabricate microelectromechanical systems (MEMS) with anisotropic mechanical and tunable fluid-phase processing. The resulting device structures had fracture sizes of 6 μm.[167] These kinds of MEMS (Figure 13)

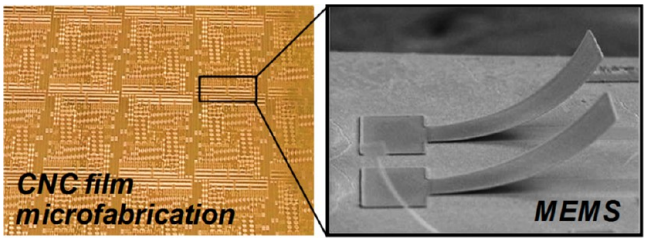

Figure 13. Photograph depicting the use of shear-aligned CNCs to fabricate microelectromechanical systems (MEMS). Reproduced from ref 167. Copyright 2018 American Chemical Society.

will find immense applications including medical, transportation, and communication products. Wet spun fibers were developed by mixing sodium alginate solution with CNCs.[168] The mechanical properties of the resulting fibers are highly influenced mainly by the degree of alignment of the CNCs, and these fibers could be used for applications such as wound dressing, drug delivery, etc. Fe_3O_4/aligned CNCs were incorporated as a reinforcing filler for rubber to create anisotropic rubber nanocomposites.[169] Under low magnetic fields, CNCs were aligned in an epoxidized natural rubber (ENR) matrix. Compared with the neat ENR, the aligned nanocomposite showed a higher modulus and increment in tensile strength. An attempt to biomimic natural silkworm silk using a silk fibroin (SF) matrix incorporated with CNCs was successfully carried out by Liu et al.[170] via wet-spinning assembly technology. Circular-shaped resultant fibers with dense morphology had CNCs aligned along the fiber axis. CNC-induced orientation and crystallization along with the strong hydrogen-bonding interactions have been found to be the main factors contributing to enhanced properties of the SF matrix.

A potential application of CNCs as scaffolds for tissue engineering was demonstrated by He et al.[171] Directed cellular organization was observed on the scaffolds prepared by electrospinning (Figure 14), resulting in well-oriented CNCs with cellulose nanofibers (aligned uniaxially). Such scaffolds with unique cell orientation will have high utility in making organs such as tendon, nerve, and artificial tissues. Bio-based scaffolds with controllable pore structures were fabricated

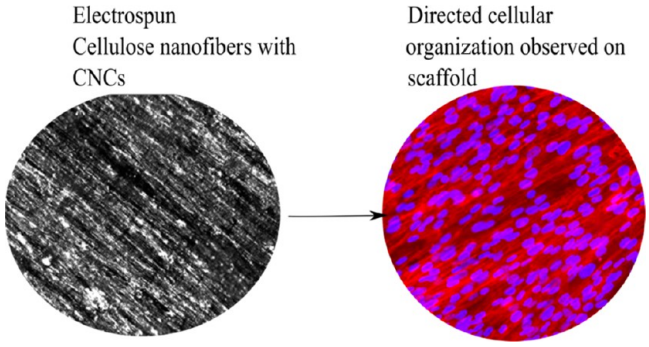

Figure 14. (left) Polarized light microscopy image of electrospun cellulose nanofibers with CNCs. (right) Confocal laser scanning microscopy image of the same fibers loaded with human dental follicle cells. Adapted from ref 171. Copyright 2014 American Chemical Society.

using 3D printing of a cross-linked polymer network comprising CNC-reinforced sodium alginate and gelatin.[172] CNCs get aligned along the printing direction and facilitate 3D printing of the polymer matrix by providing favorable rheological properties. Such gradient pore structures with nanoscale pore wall roughness facilitate optimal tissue regeneration. In vivo cortical bone regeneration and collagen assembly along with differentiation of human mesenchymal stem cells (BMSCs) in vitro were investigated using bone morphogenetic protein-2 (BMP-2)-loaded fibers of aligned electrospun CNC/cellulose nanocomposite.[173] Good biocompatibility was observed with such scaffolds, wherein alignment of the cellulose fiber morphology governed the growth orientation of the BMSCs. Magnetically aligned CNC-based composite hydrogels were used to assess in vivo subcutaneous tissue responses, protein adsorption, and cell adhesion in vitro.[174] A significant increment in cell adhesion was observed with CNC loading, whereas protein adsorption had minimal impact. These magnetically aligned hydrogels showed significant fibroblast penetration irrespective of chronic and mild acute inflammatory responses.

Zhao et al.[175] developed a uniform and scalable CNC microfilm (Figure 15a), that showed efficient photonic property and was suggested to have potential utility in interactive pigments and cosmetic applications. The exceptionally consistent optical microfilms were prepared from discrete nanoliter sessile droplets. Biosourced photonic films with a chiral optical response were fabricated using aligned CNC films, which were oriented using 0.5−1.2 T magnets to tune in suspension before assembling into films.[176] Sustainable photonic pigments in cosmetics, security labeling, and coatings employ matte textures developed from these iridescent films with powerful visual appearance. Naked-eye qualitative detectability of vapors, a practical application for chemical sensors, was successfully demonstrated using optical coatings with layer-by-layer film stacking of CNCs.[177] The nanorods were aligned in the direction of axial centrifugation. By adjustment of the layer deposition, transition of reflected colors from blue to orange could be tuned or monitored. An irreversible color variation at room temperature was observed when vapors diffused into the coating surface. This irreversible color response was highly dependent on chemical interface interaction and diffusion of vapors into the coating. Chiral CNC solid films with highly oriented layered morphology were bioderived from a thin-capillary-bound CNC suspension

https://dx.doi.org/10.1021/acsabm.0c00104
ACS Appl. Bio Mater. 2020, 3, 1828−1844

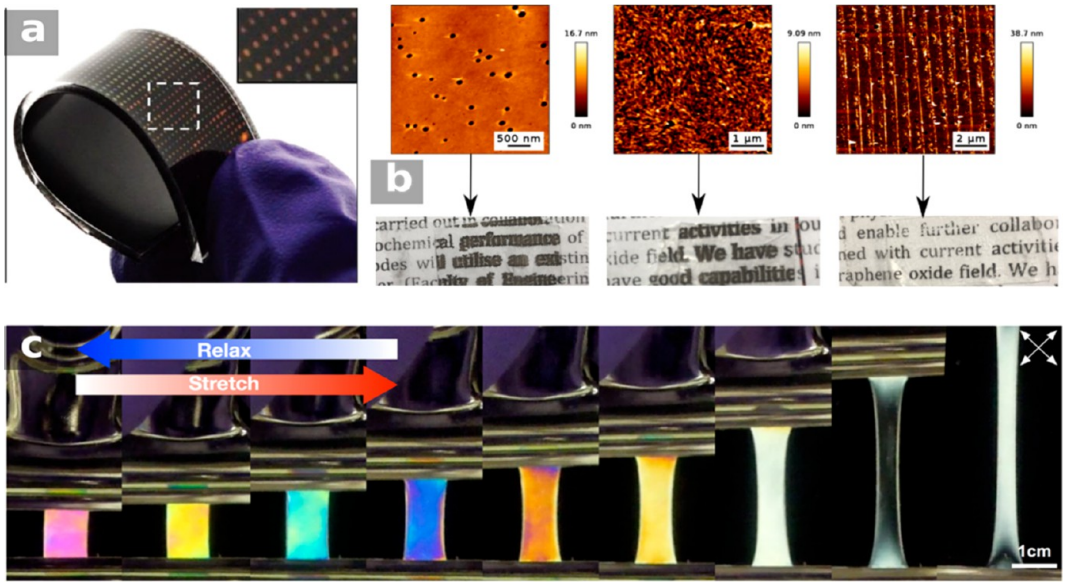

Figure 15. (a) Photograph of a flexible PDMS substrate with a CNC microfilm array. From ref 175. CC BY 4.0. (b) Upper left to right shows the AFM images of polystyrene, polystyrene coated with random CNCs, and polystyrene coated with aligned CNCs. Their corresponding utility in ink printing is depicted in the bottom images, which evidently show that aligned-CNC-coated PS prevents ink bleeding. Reproduced from ref 183. Copyright 2019 American Chemical Society. (c) Cross-polarized photographs of CNC/elastomer composite samples showing interference colors when elongated perpendicular to the direction of CNC alignment. Reproduced from ref 185. Copyright 2019 American Chemical Society.

(liquid-crystal phase).[178] The interface between chiral and isotropic phases was aligned perpendicular to the long capillary axis because the drying process was confined by the capillary space. The uniform layer morphology was obtained as a result of a unidirectional anisotropic phase, promoted by the anisotropic drying of water vapor in one saturated capillary end. Uniform birefringence and a narrow optical reflectance band were observed in the resultant chiral CNC films, opening the door to several applications in bioderived photonic nanomaterials due to the uniform morphology and structural color. Surfactant-modified CNCs blended with PLA were extruded into films wherein CNCs were aligned during extrusion (self-assembly).[179] The films showed intricate colors due to the aligned assembly of CNCs at high concentrations, observed between crossed polarizers. At an optimum concentration of CNCs loaded into PLA matrix, the mechanical properties of the resultant films were found to be enhanced. CNCs were surfactant-modified so as to tackle the compatibility with the PLA matrix, which is hydrophobic in nature. A simple and controllable method of producing birefringent films of CNCs was successfully carried out by dip-coating aqueous suspensions of hydrolyzed filter paper on glass substrates.[180] Preferential alignment of CNCs was facilitated by the dragging forces during film deposition. Dynamic hybrid hydrogels with multidimensional birefringence were fabricated using CNCs with hydrodynamic alignment by a shear-thinning phenomenon in the hydrogel network.[181] Once the external force is unloaded, the polymer network relaxes faster than the CNCs, thereby preserving the hydrodynamic alignment of CNCs in the relaxed hydrogel. The orientation index of the CNCs is further enhanced by the surface tension of hydrogels during the drying process, which results in anisotropic behavior with tunable birefringence. This approach facilitates the development of anisotropic microstructures of diverse xerogels like films and fibers without an external mold because of the presence of boundaries in the hydrogel network. Bioinspired films with photonic behavior were prepared that biomimic floral striations.[182] CNC films with a microscopic wrinkled surface and cholesteric organization were synthesized using nanoimprinting lithography assisted through evaporation, a molding technique that is used to cast free-standing films of CNCs onto an oriented wrinkle template. Optically tunable structural color along with short-wavelength light scattering (induced by the morphology) was observed with the resultant cellulose films. Such cholesteric cellulose films with relief-wrinkled surfaces could be controlled precisely, which could be used in creating microscopic patterned images via engineering printing.

Patterned coatings of CNCs were used to accomplish high-resolution inkjet printing (Figure 15b) on a hydrophobic polystyrene (PS) surface.[183] Uniaxially stretched PDMS was surface-oxidized using plasma to create crack-free periodic wrinkles with a wavelength of ∼850 nm. These wrinkled elastomeric substrates were spin-coated with CNCs and then stamped onto the PS surface using a tiny droplet of water, thereby creating aligned CNCs on the PS surface. A decrement in wettability was observed with aligned CNCs because the increased local surface roughness facilitated pinning at the liquid interface. When ink is printed on aligned-CNC-coated PS, the bleeding of ink is prevented, which is a traditional disadvantage of hydrophobic polymers for printing. Thus, roll-to-roll manufacturing for industrial flexoprinting could be achieved using this technology with suitable further modifications.

CNCs were aligned using a 3D printing technique wherein aqueous inks composed of CNCs and xyloglucan were freeze-cast.[184] The resultant sample reflected the internal structure of several wood species, thereby paving the way for the development of renewable wood-based materials via additive manufacturing technologies. Shear-based alignment of CNCs was incorporated into an elastomer matrix, which showed a reversible optical property when a mechanical stress was applied (Figure 15c).[185] This could be a potential application for biosensors that work on the principle of external stimuli.

https://dx.doi.org/10.1021/acsabm.0c00104
ACS Appl. Bio Mater. 2020, 3, 1828−1844

Aligned porous-structured foams with CNCs at two different freezing temperatures were developed.[186] The addition of CNCs into a poly(vinyl alcohol) foam reduced the moisture uptake. At −186 °C, a highly aligned porous foam structure was observed along the direction of ice growth. The change in freezing temperature could influence the unique features of these foams, which could be of high utility in applications such as thermal insulators and tissue engineering scaffolds. A CNC emulsion was made into a fabric by spin-coating of the CNC emulsion onto stretch-released PDMS, which is stacked together after the film is peeled off from the PDMS surface.[187] Such CNC fabric can function as a structured template to align other nanoparticles. Self-assembled CNC particles above the critical CNC concentration with chiral nematic ordering were used in water-based lubricants as additives.[188] CNC lubricants at different concentrations were used to measure the coefficient of friction and wear between a chrome steel ball and a stainless steel shaft. Alignment of CNC rods was found to improve the coefficient of friction and wear at a CNC concentration of 2 wt %.

6. CONCLUSION AND FUTURE DIRECTIONS

Cellulose nanocrystals, a natural product, provide a path for increasing sustainability in several applications, including reinforcement of polymer matrices, drug delivery applications, production of iridescent films, etc. Their abundant hydroxyl groups provide the potential for surface functionalization that can be used to tailor them for desired applications. To recapitulate, the review initially discussed the production of CNCs from primitive wood pulp and their general applications. This helped us to set up the base for the main focus of this review, where the different ways of aligning CNCs to achieve desired surface and material characteristics, quantification of the alignment using various characterization techniques, and the reported major applications of such aligned CNCs were extensively discussed. Irrespective of the applications of aligned CNCs reported, their scalability for large-scale production is still a concern, for which fundamental studies on the alignment of CNCs need to be explored in more depth. Cost effectiveness with minimum resource utilization should be the ultimate goal while dealing with the end applications of aligned CNCs.

Aligned CNCs as a template to grow muscle cells in a unidirectional manner provide a great insight into incorporating CNC alignment into biomedical applications. Although the biocompatibility of cellulose nanocrystals offers potential for aligning cells, it is also a challenging avenue for future investigation. For this we would require a large surface with aligned CNC features, as the cell dimensions are normally in the micrometer range instead of the nanometer range. Also, wrinkle-free alignment methods could be used to make graphene oxide (GO)/CNC composite materials wherein aligned CNCs could be stamped over GO layers followed by reduction of the GO using methods such as laser reduction. This would enable the formation of unidirectional conductive surfaces. Bridging between CNCs and GO could be facilitated using simple ionic salts like calcium chloride. In addition, the use of aligned CNCs for water droplet capture and retention, due to its high average critical roll-off angle, could be explored in future studies.

Another interesting aspect will be to investigate hierarchical CNC structures for photonic applications. As an alternative to the conventional PDMS wrinkling process (CNCs deposited after wrinkling of PDMS), we could also try to deposit CNCs on nonwrinkled PDMS using spin-coating and then wrinkle the PDMS/CNC material to see whether CNCs are aligned better than with the conventional method, avoiding potential pitfalls of the current method. The use of aligned CNCs to detect and sense biomolecules could be explored, along with using the structure color generated from CNC alignment to sense mechanical stress, all of which would contribute to the development of flexible and wearable natural biosensors. These future perspectives could also be applied with other forms of cellulose such as cellulose nanofibers, bacterial cellulose, surface-functionalized cellulose, etc., which are aligned in different ways similar to what we have discussed for cellulose nanocrystals.

AUTHOR INFORMATION

Corresponding Author

Jinguang Hu − *Department of Chemical and Petroleum Engineering, University of Calgary, Calgary, AB T2N 1N4, Canada;* orcid.org/0000-0001-8033-7102; Email: jinguang.hu@ucalgary.ca

Authors

Ragesh Prathapan − *Department of Chemical and Petroleum Engineering, University of Calgary, Calgary, AB T2N 1N4, Canada*

Rico F. Tabor − *School of Chemistry, Monash University, Clayton, VIC 3800, Australia;* orcid.org/0000-0003-2926-0095

Gil Garnier − *Bioresources Processing Research Institute of Australia (BioPRIA), Department of Chemical Engineering, Monash University, Clayton, VIC 3800, Australia;* orcid.org/0000-0003-3512-0056

Complete contact information is available at: https://pubs.acs.org/10.1021/acsabm.0c00104

Notes

The authors declare no competing financial interest.

ACKNOWLEDGMENTS

This research was undertaken thanks in part to funding from the Canada First Research Excellence Fund (CFREF). The authors acknowledge the University of Calgary and Monash University for the joint collaborative network.

ABBREVIATIONS

MFC, microfibrillated cellulose; NFC, nanofibrillated cellulose; CNC, cellulose nanocrystal; TEM, transmission electron microscopy; SEM, scanning electron microscopy; MCC, microcrystalline cellulose; PLA, poly(lactic acid); EPTMAC, epoxypropyl trimethylammonium chloride; AFM, atomic force microscopy; PFC, parabolic focal conic; GIWAXS, grazing-incidence wide-angle X-ray scattering; DC, direct current; AC, alternating current; GO, graphene oxide; PVA, poly(vinyl acetate); LB, Langmuir−Blodgett; LS, Langmuir−Schaeffer; PDMS, poly(dimethylsiloxane); PEI, poly(ethylenimine); XRD, X-ray diffraction; PSD, power spectral density; WAXD, wide-angle X-ray diffraction; SAXS, small-angle X-ray scattering; MEMS, microelectromechanical systems; SF, silk fibroin; BMSCs, bone marrow-derived mesenchymal stem cells; BMP-2, bone morphogenetic protein-2; PS, polystyrene

https://dx.doi.org/10.1021/acsabm.0c00104
ACS Appl. Bio Mater. 2020, 3, 1828−1844

REFERENCES

(1) Dufresne, A. Nanocellulose: From Nature to High Performance Tailored Materials. De Gruyter, 2012. DOI: 10.1515/9783110254600

(2) Thomas, B.; Raj, M. C.; B, A. K.; H, R. M.; Joy, J.; Moores, A.; Drisko, G. L.; Sanchez, C. Nanocellulose, a Versatile Green Platform: From Biosources to Materials and Their Applications. *Chem. Rev.* **2018**, *118* (24), 11575−11625.

(3) De France, K. J.; Hoare, T.; Cranston, E. D. Review of Hydrogels and Aerogels Containing Nanocellulose. *Chem. Mater.* **2017**, *29* (11), 4609−4631.

(4) Kim, J.-H.; Lee, D.; Lee, Y.-H.; Chen, W.; Lee, S.-Y. Nanocellulose for Energy Storage Systems: Beyond the Limits of Synthetic Materials. *Adv. Mater.* **2019**, *31* (20), 1804826.

(5) Chen, W.; Yu, H.; Lee, S.-Y.; Wei, T.; Li, J.; Fan, Z. Nanocellulose: A Promising Nanomaterial for Advanced Electrochemical Energy Storage. *Chem. Soc. Rev.* **2018**, *47* (8), 2837−2872.

(6) Abdul Rashid, E. S.; Muhd Julkapli, N.; Yehye, W. A. Nanocellulose Reinforced as Green Agent in Polymer Matrix Composites Applications. *Polym. Adv. Technol.* **2018**, *29* (6), 1531−1546.

(7) Fratzl, P.; Burgert, I.; Gupta, H. S. On the Role of Interface Polymers for the Mechanics of Natural Polymeric Composites. *Phys. Chem. Chem. Phys.* **2004**, *6* (24), 5575−5579.

(8) Studart, A. R. Towards High-Performance Bioinspired Composites. *Adv. Mater.* **2012**, *24* (37), 5024−5044.

(9) Barthelat, F.; Yin, Z.; Buehler, M. J. Structure and Mechanics of Interfaces in Biological Materials. *Nat. Rev. Mater.* **2016**, *1* (4), 16007.

(10) Hamedi, M. M.; Hajian, A.; Fall, A. B.; Håkansson, K.; Salajkova, M.; Lundell, F.; Wågberg, L.; Berglund, L. A. Highly Conducting, Strong Nanocomposites Based on Nanocellulose-Assisted Aqueous Dispersions of Single-Wall Carbon Nanotubes. *ACS Nano* **2014**, *8* (3), 2467−2476.

(11) Tang, Z.; Kotov, N. A.; Magonov, S.; Ozturk, B. Nanostructured Artificial Nacre. *Nat. Mater.* **2003**, *2* (6), 413−418.

(12) Wegst, U. G. K.; Bai, H.; Saiz, E.; Tomsia, A. P.; Ritchie, R. O. Bioinspired Structural Materials. *Nat. Mater.* **2015**, *14* (1), 23−36.

(13) Teeri, T. T.; Brumer, H.; Daniel, G.; Gatenholm, P. Biomimetic Engineering of Cellulose-Based Materials. *Trends Biotechnol.* **2007**, *25* (7), 299−306.

(14) Nimz, H. H. Wood-Chemistry, Ultrastructure, Reactions. *Holz als Roh- und Werkst.* **1984**, *42* (8), 314.

(15) Yang, H.; Yan, R.; Chen, H.; Lee, D. H.; Zheng, C. Characteristics of Hemicellulose, Cellulose and Lignin Pyrolysis. *Fuel* **2007**, *86* (12−13), 1781−1788.

(16) Marchessault, R. H.; Malhotra, S. L.; Jones, A. Y.; Perovic, A. The Wood Explosion Process: Characterization and Uses of Lignin/Cellulose Products. In *Wood and Agricultural Residues*; Soltes, E. J., Ed.; Academic Press, 1983; pp 401−413. DOI: 10.1016/B978-0-12-654560-9.50026-3

(17) Chang, T.-C.; Chang, H.-T.; Wu, C.-L.; Chang, S.-T. Influences of Extractives on the Photodegradation of Wood. *Polym. Degrad. Stab.* **2010**, *95* (4), 516−521.

(18) Gralén, N.; Svedberg, T. Molecular Weight of Native Cellulose. *Nature* **1943**, *152* (3865), 625.

(19) Habibi, Y.; Lucia, L. A.; Rojas, O. J. Cellulose Nanocrystals: Chemistry, Self-Assembly, and Applications. *Chem. Rev.* **2010**, *110* (6), 3479−3500.

(20) Huang, Z.; Raghuwanshi, V. S.; Garnier, G. Functionality of Immunoglobulin G and Immunoglobulin M Antibody Physisorbed on Cellulosic Films. *Front. Bioeng. Biotechnol.* **2017**, *5*, 41.

(21) Atalla, R. H.; Vanderhart, D. L. Native Cellulose: A Composite of Two Distinct Crystalline Forms. *Science* **1984**, *223* (4633), 283−285.

(22) Turbak, A. F.; Snyder, F. W.; Sandberg, K. R. Microfibrillated Cellulose, a New Cellulose Product: Properties, Uses, and Commercial Potential. *J. Appl. Polym. Sci.: Appl. Polym. Symp.* **1983**, *37*, 815−827.

(23) Klemm, D.; Kramer, F.; Moritz, S.; Lindström, T.; Ankerfors, M.; Gray, D.; Dorris, A. Nanocelluloses: A New Family of Nature-Based Materials. *Angew. Chem., Int. Ed.* **2011**, *50* (24), 5438−5466.

(24) Wågberg, L.; Decher, G.; Norgren, M.; Lindström, T.; Ankerfors, M.; Axnäs, K. The Build-Up of Polyelectrolyte Multilayers of Microfibrillated Cellulose and Cationic Polyelectrolytes. *Langmuir* **2008**, *24* (3), 784−795.

(25) Nishiyama, Y.; Sugiyama, J.; Chanzy, H.; Langan, P. Crystal Structure and Hydrogen Bonding System in Cellulose Iα from Synchrotron X-ray and Neutron Fiber Diffraction. *J. Am. Chem. Soc.* **2003**, *125* (47), 14300−14306.

(26) Nishiyama, Y.; Langan, P.; Chanzy, H. Crystal Structure and Hydrogen-Bonding System in Cellulose Iβ from Synchrotron X-ray and Neutron Fiber Diffraction. *J. Am. Chem. Soc.* **2002**, *124* (31), 9074−9082.

(27) Williams, G. I.; Wool, R. P. Composites from Natural Fibers and Soy Oil Resins. *Appl. Compos. Mater.* **2000**, *7* (5), 421−432.

(28) Van de Velde, K.; Kiekens, P. Thermoplastic Pultrusion of Natural Fibre Reinforced Composites. *Compos. Struct.* **2001**, *54* (2−3), 355−360.

(29) Bledzki, A. K.; Gassan, J. Einfluß von Haftvermittlern auf das Feuchteverhalten Naturfaserverstärkter Kunststoffe. *Angew. Makromol. Chem.* **1996**, *236* (1), 129−138.

(30) Alemdar, A.; Sain, M. Biocomposites from Wheat Straw Nanofibers: Morphology, Thermal and Mechanical Properties. *Compos. Sci. Technol.* **2008**, *68* (2), 557−565.

(31) Zimmermann, T.; Bordeanu, N.; Strub, E. Properties of Nanofibrillated Cellulose from Different Raw Materials and Its Reinforcement Potential. *Carbohydr. Polym.* **2010**, *79* (4), 1086−1093.

(32) Wang, B.; Sain, M. Dispersion of Soybean Stock-Based Nanofiber in a Plastic Matrix. *Polym. Int.* **2007**, *56* (4), 538−546.

(33) Kalia, S.; Kaith, B. S.; Kaur, I. Pretreatments of Natural Fibers and Their Application as Reinforcing Material in Polymer Composites—A Review. *Polym. Eng. Sci.* **2009**, *49* (7), 1253−1272.

(34) Kalia, S.; Kaith, B. S.; Sharma, S.; Bhardwaj, B. Mechanical Properties of Flax-g-Poly(Methyl Acrylate) Reinforced Phenolic Composites. *Fibers Polym.* **2008**, *9* (4), 416−422.

(35) Sreekala, M. S.; Kumaran, M. G.; Joseph, S.; Jacob, M.; Thomas, S. Oil Palm Fibre Reinforced Phenol Formaldehyde Composites: Influence of Fibre Surface Modifications on the Mechanical Performance. *Appl. Compos. Mater.* **2000**, *7* (5), 295−329.

(36) Ray, D.; Sarkar, B. K.; Rana, A. K.; Bose, N. R. Effect of Alkali Treated Jute Fibres on Composite Properties. *Bull. Mater. Sci.* **2001**, *24* (2), 129−135.

(37) Eichhorn, S. J.; Dufresne, A.; Aranguren, M.; Marcovich, N. E.; Capadona, J. R.; Rowan, S. J.; Weder, C.; Thielemans, W.; Roman, M.; Renneckar, S.; Gindl, W.; Veigel, S.; Keckes, J.; Yano, H.; Abe, K.; Nogi, M.; Nakagaito, A. N.; Mangalam, A.; Simonsen, J.; Benight, A. S.; Bismarck, A.; Berglund, L. A.; Peijs, T. Review: Current International Research into Cellulose Nanofibres and Nanocomposites. *J. Mater. Sci.* **2010**, *45* (1), 1−33.

(38) Pommet, M.; Juntaro, J.; Heng, J. Y. Y.; Mantalaris, A.; Lee, A. F.; Wilson, K.; Kalinka, G.; Shaffer, M. S. P.; Bismarck, A. Surface Modification of Natural Fibers Using Bacteria: Depositing Bacterial Cellulose onto Natural Fibers To Create Hierarchical Fiber Reinforced Nanocomposites. *Biomacromolecules* **2008**, *9* (6), 1643−1651.

(39) Shoda, M.; Sugano, Y. Recent Advances in Bacterial Cellulose Production. *Biotechnol. Bioprocess Eng.* **2005**, *10* (1), 1.

(40) Eichhorn, S. J. Cellulose Nanowhiskers: Promising Materials for Advanced Applications. *Soft Matter* **2011**, *7* (2), 303−315.

(41) Kumar, A.; Negi, Y. S.; Choudhary, V.; Bhardwaj, N. K. Characterization of Cellulose Nanocrystals Produced by Acid-Hydrolysis from Sugarcane Bagasse as Agro-Waste. *J. Mater. Phys. Chem.* **2014**, *2* (1), 1−8.

(42) Koshizawa, T. Degradation of Wood Cellulose and Cotton Linters in Phosphoric Acid. *Kami Pa Gikyoshi* **1960**, *14* (7), 455−458,475.

https://dx.doi.org/10.1021/acsabm.0c00104
ACS Appl. Bio Mater. 2020, 3, 1828−1844

(43) Usuda, M.; Suzuki, O.; Nakano, J.; Migita, N. Acid Hydrolysis of Cellulose in Concentrated Phosphoric Acid; Influences of Modified Groups of Cellulose on the Rate of Hy Drolysis. *J. Soc. Chem. Ind. Japan* **1967**, *70* (3), 349−352.
(44) Sadeghifar, H.; Filpponen, I.; Clarke, S. P.; Brougham, D. F.; Argyropoulos, D. S. Production of Cellulose Nanocrystals Using Hydrobromic Acid and Click Reactions on Their Surface. *J. Mater. Sci.* **2011**, *46* (22), 7344−7355.
(45) Araki, J.; Wada, M.; Kuga, S.; Okano, T. Influence of Surface Charge on Viscosity Behavior of Cellulose Microcrystal Suspension. *J. Wood Sci.* **1999**, *45* (3), 258−261.
(46) Roman, M.; Winter, W. T. Effect of Sulfate Groups from Sulfuric Acid Hydrolysis on the Thermal Degradation Behavior of Bacterial Cellulose. *Biomacromolecules* **2004**, *5* (5), 1671−1677.
(47) Wang, N.; Ding, E.; Cheng, R. Preparation and Liquid Crystalline Properties of Spherical Cellulose Nanocrystals. *Langmuir* **2008**, *24* (1), 5−8.
(48) Wang, N.; Ding, E.; Cheng, R. Thermal Degradation Behaviors of Spherical Cellulose Nanocrystals with Sulfate Groups. *Polymer* **2007**, *48* (12), 3486−3493.
(49) Bondeson, D.; Mathew, A.; Oksman, K. Optimization of the Isolation of Nanocrystals from Microcrystalline Celluloseby Acid Hydrolysis. *Cellulose* **2006**, *13* (2), 171.
(50) Sain, M.; Oksman, K. Introduction to Cellulose Nanocomposites. *Cellulose Nanocomposites* **2006**, *938*, 2−8.
(51) Dong, X. U. E. M. I. N.; Revol, J.-F.; Gray, D. G. Effect of Microcrystallite Preparation Conditions on the Formation of Colloid Crystals of Cellulose. *Cellulose* **1998**, *5* (1), 19−32.
(52) Lu, P.; Hsieh, Y.-L. Preparation and Properties of Cellulose Nanocrystals: Rods, Spheres, and Network. *Carbohydr. Polym.* **2010**, *82* (2), 329−336.
(53) Li, W.; Yue, J.; Liu, S. Preparation of Nanocrystalline Cellulose via Ultrasound and Its Reinforcement Capability for Poly(Vinyl Alcohol) Composites. *Ultrason. Sonochem.* **2012**, *19* (3), 479−485.
(54) Cui, S.; Zhang, S.; Ge, S.; Xiong, L.; Sun, Q. Green Preparation and Characterization of Size-Controlled Nanocrystalline Cellulose via Ultrasonic-Assisted Enzymatic Hydrolysis. *Ind. Crops Prod.* **2016**, *83*, 346−352.
(55) Tang, Y.; Yang, S.; Zhang, N.; Zhang, J. Preparation and Characterization of Nanocrystalline Cellulose via Low-Intensity Ultrasonic-Assisted Sulfuric Acid Hydrolysis. *Cellulose* **2014**, *21* (1), 335−346.
(56) Guo, J.; Guo, X.; Wang, S.; Yin, Y. Effects of Ultrasonic Treatment during Acid Hydrolysis on the Yield, Particle Size and Structure of Cellulose Nanocrystals. *Carbohydr. Polym.* **2016**, *135*, 248−255.
(57) Li, W.; Wang, R.; Liu, S. Nanocrystalline Cellulose Prepared From Softwood Kraft Pulp via Ultrasonic-Assisted Acid Hydrolysis. *BioResources* **2011**, *6* (4), 4271−4281.
(58) Lu, Q.; Tang, L.; Lin, F.; Wang, S.; Chen, Y.; Chen, X.; Huang, B. Preparation and Characterization of Cellulose Nanocrystals via Ultrasonication-Assisted FeCl3-Catalyzed Hydrolysis. *Cellulose* **2014**, *21* (5), 3497−3506.
(59) Yu, H.; Qin, Z.; Liang, B.; Liu, N.; Zhou, Z.; Chen, L. Facile Extraction of Thermally Stable Cellulose Nanocrystals with a High Yield of 93% through Hydrochloric Acid Hydrolysis under Hydrothermal Conditions. *J. Mater. Chem. A* **2013**, *1* (12), 3938−3944.
(60) Camarero Espinosa, S.; Kuhnt, T.; Foster, E. J.; Weder, C. Isolation of Thermally Stable Cellulose Nanocrystals by Phosphoric Acid Hydrolysis. *Biomacromolecules* **2013**, *14* (4), 1223−1230.
(61) Mohd Amin, K. N.; Annamalai, P. K.; Morrow, I. C.; Martin, D. Production of Cellulose Nanocrystals via a Scalable Mechanical Method. *RSC Adv.* **2015**, *5* (70), 57133−57140.
(62) Favier, V.; Chanzy, H.; Cavaille, J. Y. Polymer Nanocomposites Reinforced by Cellulose Whiskers. *Macromolecules* **1995**, *28* (18), 6365−6367.
(63) Azizi Samir, M. A. S.; Alloin, F.; Sanchez, J.-Y.; Dufresne, A. Cellulose Nanocrystals Reinforced Poly(Oxyethylene). *Polymer* **2004**, *45* (12), 4149−4157.
(64) Azizi Samir, M. A. S.; Chazeau, L.; Alloin, F.; Cavaillé, J.-Y.; Dufresne, A.; Sanchez, J.-Y. POE-Based Nanocomposite Polymer Electrolytes Reinforced with Cellulose Whiskers. *Electrochim. Acta* **2005**, *50* (19), 3897−3903.
(65) Junior de Menezes, A.; Siqueira, G.; Curvelo, A. A. S.; Dufresne, A. Extrusion and Characterization of Functionalized Cellulose Whiskers Reinforced Polyethylene Nanocomposites. *Polymer* **2009**, *50* (19), 4552−4563.
(66) Qi, H.; Cai, J.; Zhang, L.; Kuga, S. Properties of Films Composed of Cellulose Nanowhiskers and a Cellulose Matrix Regenerated from Alkali/Urea Solution. *Biomacromolecules* **2009**, *10* (6), 1597−1602.
(67) Petersson, L.; Mathew, A. P.; Oksman, K. Dispersion and Properties of Cellulose Nanowhiskers and Layered Silicates in Cellulose Acetate Butyrate Nanocomposites. *J. Appl. Polym. Sci.* **2009**, *112* (4), 2001−2009.
(68) Dong, S.; Roman, M. Fluorescently Labeled Cellulose Nanocrystals for Bioimaging Applications. *J. Am. Chem. Soc.* **2007**, *129* (45), 13810−13811.
(69) Auad, M. L.; Mosiewicki, M. A.; Richardson, T.; Aranguren, M. I.; Marcovich, N. E. Nanocomposites Made from Cellulose Nanocrystals and Tailored Segmented Polyurethanes. *J. Appl. Polym. Sci.* **2010**, *115* (2), 1215−1225.
(70) Kvien, I.; Tanem, B. S.; Oksman, K. Characterization of Cellulose Whiskers and Their Nanocomposites by Atomic Force and Electron Microscopy. *Biomacromolecules* **2005**, *6* (6), 3160−3165.
(71) Pandey, J. K.; Lee, C. S.; Ahn, S.-H. Preparation and Properties of Bio-Nanoreinforced Composites from Biodegradable Polymer Matrix and Cellulose Whiskers. *J. Appl. Polym. Sci.* **2010**, *115* (4), 2493−2501.
(72) Shanmuganathan, K.; Capadona, J. R.; Rowan, S. J.; Weder, C. Bio-Inspired Mechanically-Adaptive Nanocomposites Derived from Cotton Cellulose Whiskers. *J. Mater. Chem.* **2010**, *20* (1), 180−186.
(73) Liu, H.; Liu, D.; Yao, F.; Wu, Q. Fabrication and Properties of Transparent Polymethylmethacrylate/Cellulose Nanocrystals Composites. *Bioresour. Technol.* **2010**, *101* (14), 5685−5692.
(74) de Mesquita, J. P.; Donnici, C. L.; Pereira, F. V. Biobased Nanocomposites from Layer-by-Layer Assembly of Cellulose Nanowhiskers with Chitosan. *Biomacromolecules* **2010**, *11* (2), 473−480.
(75) Wang, H.; Roman, M. Formation and Properties of Chitosan−Cellulose Nanocrystal Polyelectrolyte−Macroion Complexes for Drug Delivery Applications. *Biomacromolecules* **2011**, *12* (5), 1585−1593.
(76) Jackson, J. K.; Letchford, K.; Wasserman, B. Z.; Ye, L.; Hamad, W. Y.; Burt, H. M. The Use of Nanocrystalline Cellulose for the Binding and Controlled Release of Drugs. *Int. J. Nanomed.* **2011**, *6*, 321−330.
(77) Dong, S.; Cho, H. J.; Lee, Y. W.; Roman, M. Synthesis and Cellular Uptake of Folic Acid-Conjugated Cellulose Nanocrystals for Cancer Targeting. *Biomacromolecules* **2014**, *15* (5), 1560−1567.
(78) Hasani, M.; Cranston, E. D.; Westman, G.; Gray, D. G. Cationic Surface Functionalization of Cellulose Nanocrystals. *Soft Matter* **2008**, *4* (11), 2238−2244.
(79) Salajková, M.; Berglund, L. A.; Zhou, Q. Hydrophobic Cellulose Nanocrystals Modified with Quaternary Ammonium Salts. *J. Mater. Chem.* **2012**, *22* (37), 19798−19805.
(80) Yuan, H.; Nishiyama, Y.; Wada, M.; Kuga, S. Surface Acylation of Cellulose Whiskers by Drying Aqueous Emulsion. *Biomacromolecules* **2006**, *7* (3), 696−700.
(81) Habibi, Y.; Chanzy, H.; Vignon, M. R. TEMPO-Mediated Surface Oxidation of Cellulose Whiskers. *Cellulose* **2006**, *13* (6), 679−687.
(82) Jasmani, L.; Eyley, S.; Schütz, C.; Van Gorp, H.; De Feyter, S.; Thielemans, W. One-Pot Functionalization of Cellulose Nanocrystals with Various Cationic Groups. *Cellulose* **2016**, *23* (6), 3569−3576.
(83) Eyley, S.; Thielemans, W. Surface Modification of Cellulose Nanocrystals. *Nanoscale* **2014**, *6* (14), 7764−7779.
(84) Folda, T.; Hoffmann, H.; Chanzy, H.; Smith, P. Liquid Crystalline Suspensions of Poly(Tetrafluoroethylene) "Whiskers. *Nature* **1988**, *333* (6168), 55−56.

https://dx.doi.org/10.1021/acsabm.0c00104
ACS Appl. Bio Mater. 2020, 3, 1828−1844

(85) Oster, G. Two-Phase Formation in Solutions of Tobacco Mosaic Virus and the Problem of Long-Range Forces. *J. Gen. Physiol.* **1950**, *33* (5), 445−473.
(86) Livolant, F.; Leforestier, A. Condensed Phases of DNA: Structures and Phase Transitions. *Prog. Polym. Sci.* **1996**, *21* (6), 1115−1164.
(87) Revol, J.-F.; Bradford, H.; Giasson, J.; Marchessault, R. H.; Gray, D. G. Helicoidal Self-Ordering of Cellulose Microfibrils in Aqueous Suspension. *Int. J. Biol. Macromol.* **1992**, *14* (3), 170−172.
(88) Araki, J.; Kuga, S. Effect of Trace Electrolyte on Liquid Crystal Type of Cellulose Microcrystals. *Langmuir* **2001**, *17* (15), 4493−4496.
(89) Araki, J.; Wada, M.; Kuga, S.; Okano, T. Birefringent Glassy Phase of a Cellulose Microcrystal Suspension. *Langmuir* **2000**, *16* (6), 2413−2415.
(90) Viet, D.; Beck-Candanedo, S.; Gray, D. G. Dispersion of Cellulose Nanocrystals in Polar Organic Solvents. *Cellulose* **2007**, *14* (2), 109−113.
(91) Revol, J.-F.; Marchessault, R. H. In Vitro Chiral Nematic Ordering of Chitin Crystallites. *Int. J. Biol. Macromol.* **1993**, *15* (6), 329−335.
(92) Heux, L.; Chauve, G.; Bonini, C. Nonflocculating and Chiral-Nematic Self-Ordering of Cellulose Microcrystals Suspensions in Nonpolar Solvents. *Langmuir* **2000**, *16* (21), 8210−8212.
(93) Beck, S.; Bouchard, J.; Berry, R. Controlling the Reflection Wavelength of Iridescent Solid Films of Nanocrystalline Cellulose. *Biomacromolecules* **2011**, *12* (1), 167−172.
(94) Bardet, R.; Belgacem, N.; Bras, J. Flexibility and Color Monitoring of Cellulose Nanocrystal Iridescent Solid Films Using Anionic or Neutral Polymers. *ACS Appl. Mater. Interfaces* **2015**, *7* (7), 4010−4018.
(95) Parker, R. M.; Guidetti, G.; Williams, C. A.; Zhao, T.; Narkevicius, A.; Vignolini, S.; Frka-Petesic, B. The Self-Assembly of Cellulose Nanocrystals: Hierarchical Design of Visual Appearance. *Adv. Mater.* **2018**, *30* (19), 1704477.
(96) Roman, M.; Gray, D. G. Parabolic Focal Conics in Self-Assembled Solid Films of Cellulose Nanocrystals. *Langmuir* **2005**, *21* (12), 5555−5561.
(97) Orts, W. J.; Godbout, L.; Marchessault, R. H.; Revol, J.-F. Enhanced Ordering of Liquid Crystalline Suspensions of Cellulose Microfibrils: A Small Angle Neutron Scattering Study. *Macromolecules* **1998**, *31* (17), 5717−5725.
(98) Ebeling, T.; Paillet, M.; Borsali, R.; Diat, O.; Dufresne, A.; Cavaillé, J.-Y.; Chanzy, H. Shear-Induced Orientation Phenomena in Suspensions of Cellulose Microcrystals, Revealed by Small Angle X-ray Scattering. *Langmuir* **1999**, *15* (19), 6123−6126.
(99) Chowdhury, R. A.; Peng, S. X.; Youngblood, J. Improved Order Parameter (Alignment) Determination in Cellulose Nanocrystal (CNC) Films by a Simple Optical Birefringence Method. *Cellulose* **2017**, *24* (5), 1957−1970.
(100) Haywood, A. D.; Davis, V. A. Effects of Liquid Crystalline and Shear Alignment on the Optical Properties of Cellulose Nanocrystal Films. *Cellulose* **2017**, *24* (2), 705−716.
(101) O'Connor, T. Degrees of Freedom. *Philos. Explor.* **2009**, *12* (2), 119−125.
(102) Reising, A. B.; Moon, R. J.; Youngblood, J. P. Effect of Particle Alignment on Mechanical Properties of Neat Cellulose Nanocrystal Films. *J. Sci. Technol. For. Prod. Processes* **2012**, *2* (6), 32−41.
(103) Park, J. H.; Noh, J.; Schütz, C.; Salazar-Alvarez, G.; Scalia, G.; Bergström, L.; Lagerwall, J. P. F. Macroscopic Control of Helix Orientation in Films Dried from Cholesteric Liquid-Crystalline Cellulose Nanocrystal Suspensions. *ChemPhysChem* **2014**, *15* (7), 1477−1484.
(104) Alizadehgiashi, M.; Khabibullin, A.; Li, Y.; Prince, E.; Abolhasani, M.; Kumacheva, E. Shear-Induced Alignment of Anisotropic Nanoparticles in a Single-Droplet Oscillatory Microfluidic Platform. *Langmuir* **2018**, *34* (1), 322−330.
(105) Håkansson, K. M. O.; Fall, A. B.; Lundell, F.; Yu, S.; Krywka, C.; Roth, S. V.; Santoro, G.; Kvick, M.; Prahl Wittberg, L.; Wågberg, L.; Soderberg, L. D. Hydrodynamic Alignment and Assembly of Nanofibrils Resulting in Strong Cellulose Filaments. *Nat. Commun.* **2014**, *5*, 4018.
(106) Zhou, C.; Chu, R.; Wu, R.; Wu, Q. Electrospun Polyethylene Oxide/Cellulose Nanocrystal Composite Nanofibrous Mats with Homogeneous and Heterogeneous Microstructures. *Biomacromolecules* **2011**, *12* (7), 2617−2625.
(107) Sanchez-Botero, L.; Dimov, A. V.; Li, R.; Smilgies, D.-M.; Hinestroza, J. P. In Situ and Real-Time Studies, via Synchrotron X-ray Scattering, of the Orientational Order of Cellulose Nanocrystals during Solution Shearing. *Langmuir* **2018**, *34* (18), 5263−5272.
(108) Hoeger, I.; Rojas, O. J.; Efimenko, K.; Velev, O. D.; Kelley, S. S. Ultrathin Film Coatings of Aligned Cellulose Nanocrystals from a Convective-Shear Assembly System and Their Surface Mechanical Properties. *Soft Matter* **2011**, *7* (5), 1957−1967.
(109) Pullawan, T.; Wilkinson, A. N.; Eichhorn, S. J. Influence of Magnetic Field Alignment of Cellulose Whiskers on the Mechanics of All-Cellulose Nanocomposites. *Biomacromolecules* **2012**, *13* (8), 2528−2536.
(110) Li, D.; Liu, Z.; Al-Haik, M.; Tehrani, M.; Murray, F.; Tannenbaum, R.; Garmestani, H. Magnetic Alignment of Cellulose Nanowhiskers in an All-Cellulose Composite. *Polym. Bull.* **2010**, *65* (6), 635−642.
(111) Dhar, P.; Kumar, A.; Katiyar, V. Magnetic Cellulose Nanocrystal Based Anisotropic Polylactic Acid Nanocomposite Films: Influence on Electrical, Magnetic, Thermal, and Mechanical Properties. *ACS Appl. Mater. Interfaces* **2016**, *8* (28), 18393−18409.
(112) Sugiyama, J.; Chanzy, H.; Maret, G. Orientation of Cellulose Microcrystals by Strong Magnetic Fields. *Macromolecules* **1992**, *25* (16), 4232−4234.
(113) Kimura, F.; Kimura, T.; Tamura, M.; Hirai, A.; Ikuno, M.; Horii, F. Magnetic Alignment of the Chiral Nematic Phase of a Cellulose Microfibril Suspension. *Langmuir* **2005**, *21* (5), 2034−2037.
(114) Kim, J.; Chen, Y.; Kang, K.-S.; Park, Y.-B.; Schwartz, M. Magnetic Field Effect for Cellulose Nanofiber Alignment. *J. Appl. Phys.* **2008**, *104* (9), 096104.
(115) Revol, J.-F.; Godbout, L.; Dong, X.-M.; Gray, D. G.; Chanzy, H.; Maret, G. Chiral Nematic Suspensions of Cellulose Crystallites; Phase Separation and Magnetic Field Orientation. *Liq. Cryst.* **1994**, *16* (1), 127−134.
(116) Edgar, C. D.; Gray, D. G. Induced Circular Dichroism of Chiral Nematic Cellulose Films. *Cellulose* **2001**, *8* (1), 5−12.
(117) Kvien, I.; Oksman, K. Orientation of Cellulose Nanowhiskers in Polyvinyl Alcohol. *Appl. Phys. A: Mater. Sci. Process.* **2007**, *87* (4), 641−643.
(118) Cranston, E. D.; Gray, D. G. Formation of Cellulose-Based Electrostatic Layer-by-Layer Films in a Magnetic Field. *Sci. Technol. Adv. Mater.* **2006**, *7* (4), 319−321.
(119) Yamamoto, K.; Nakayama, Y. Orientation of Carbon Nanotubes Using Electrophoresis. *Jpn. J. Appl. Phys.* **1996**, *35* (7B), L917−L918.
(120) van der Zande, B. M. I.; Koper, G. J. M.; Lekkerkerker, H. N. W. Alignment of Rod-Shaped Gold Particles by Electric Fields. *J. Phys. Chem. B* **1999**, *103* (28), 5754−5760.
(121) Kerr, J. XL. A New Relation between Electricity and Light: Dielectrified Media Birefringent. *London, Edinburgh, Dublin Philos. Mag. J. Sci.* **1875**, *50* (332), 337−348.
(122) Bordel, D.; Putaux, J.-L.; Heux, L. Orientation of Native Cellulose in an Electric Field. *Langmuir* **2006**, *22* (11), 4899−4901.
(123) Habibi, Y.; Heim, T.; Douillard, R. AC Electric Field-Assisted Assembly and Alignment of Cellulose Nanocrystals. *J. Polym. Sci., Part B: Polym. Phys.* **2008**, *46* (14), 1430−1436.
(124) Csoka, L.; Hoeger, I. C.; Peralta, P.; Peszlen, I.; Rojas, O. J. Dielectrophoresis of Cellulose Nanocrystals and Alignment in Ultrathin Films by Electric Field-Assisted Shear Assembly. *J. Colloid Interface Sci.* **2011**, *363* (1), 206−212.
(125) Frka-Petesic, B.; Jean, B.; Heux, L. First Experimental Determination of Permanent and Induced Electric Dipolar Moments

https://dx.doi.org/10.1021/acsabm.0c00104
ACS Appl. Bio Mater. 2020, 3, 1828−1844

of Colloidal Cellulose Nanocrystals Dispersed in Apolar Solvents. *APS March Meet. Abstr.* **2012**, *2012*, A51.015.
(126) Munier, P.; Gordeyeva, K.; Bergström, L.; Fall, A. B. Directional Freezing of Nanocellulose Dispersions Aligns the Rod-Like Particles and Produces Low-Density and Robust Particle Networks. *Biomacromolecules* **2016**, *17* (5), 1875−1881.
(127) Huan, S.; Liu, G.; Cheng, W.; Han, G.; Bai, L. Electrospun Poly(Lactic Acid)-Based Fibrous Nanocomposite Reinforced by Cellulose Nanocrystals: Impact of Fiber Uniaxial Alignment on Microstructure and Mechanical Properties. *Biomacromolecules* **2018**, *19* (3), 1037−1046.
(128) Song, W.; Liu, D.; Prempeh, N.; Song, R. Fiber Alignment and Liquid Crystal Orientation of Cellulose Nanocrystals in the Electrospun Nanofibrous Mats. *Biomacromolecules* **2017**, *18* (10), 3273−3279.
(129) Cranston, E. D.; Gray, D. G. Birefringence in Spin-Coated Films Containing Cellulose Nanocrystals. *Colloids Surf., A* **2008**, *325* (1), 44−51.
(130) Lefebvre, J.; Gray, D. G. AFM of Adsorbed Polyelectrolytes on Cellulose I Surfaces Spin-Coated on Silicon Wafers. *Cellulose* **2005**, *12* (2), 127−134.
(131) Dugan, J. M.; Gough, J. E.; Eichhorn, S. J. Directing the Morphology and Differentiation of Skeletal Muscle Cells Using Oriented Cellulose Nanowhiskers. *Biomacromolecules* **2010**, *11* (9), 2498−2504.
(132) Cranston, E. D.; Gray, D. G. Morphological and Optical Characterization of Polyelectrolyte Multilayers Incorporating Nanocrystalline Cellulose. *Biomacromolecules* **2006**, *7* (9), 2522−2530.
(133) Jean, B.; Dubreuil, F.; Heux, L.; Cousin, F. Structural Details of Cellulose Nanocrystals/Polyelectrolytes Multilayers Probed by Neutron Reflectivity and AFM. *Langmuir* **2008**, *24* (7), 3452−3458.
(134) Habibi, Y.; Hoeger, I.; Kelley, S. S.; Rojas, O. J. Development of Langmuir−Schaeffer Cellulose Nanocrystal Monolayers and Their Interfacial Behaviors. *Langmuir* **2010**, *26* (2), 990−1001.
(135) Habibi, Y.; Foulon, L.; Aguié-Béghin, V.; Molinari, M.; Douillard, R. Langmuir−Blodgett Films of Cellulose Nanocrystals: Preparation and Characterization. *J. Colloid Interface Sci.* **2007**, *316* (2), 388−397.
(136) Lu, C.; Möhwald, H.; Fery, A. A Lithography-Free Method for Directed Colloidal Crystal Assembly Based on Wrinkling. *Soft Matter* **2007**, *3* (12), 1530−1536.
(137) Schweikart, A.; Horn, A.; Böker, A.; Fery, A. Controlled Wrinkling as a Novel Method for the Fabrication of Patterned Surfaces. In *Complex Macromolecular Systems I*; Müller, A. H. E., Schmidt, H.-W., Eds.; Springer: Berlin, 2010; pp 75−99. DOI: 10.1007/12_2009_22
(138) Nyström, G.; Fall, A. B.; Carlsson, L.; Wågberg, L. Aligned Cellulose Nanocrystals and Directed Nanoscale Deposition of Colloidal Spheres. *Cellulose* **2014**, *21* (3), 1591−1599.
(139) Prathapan, R.; Berry, J. D.; Fery, A.; Garnier, G.; Tabor, R. F. Decreasing the Wettability of Cellulose Nanocrystal Surfaces Using Wrinkle-Based Alignment. *ACS Appl. Mater. Interfaces* **2017**, *9* (17), 15202−15211.
(140) Goldstein, J. I.; Newbury, D. E.; Echlin, P.; Joy, D. C.; Fiori, C.; Lifshin, E. *Scanning Electron Microscopy and X-ray Microanalysis: A Text for Biologists, Materials Scientists, and Geologists*; Plenum: New York, 1981.
(141) Binnig, G.; Quate, C. F.; Gerber, C. Atomic Force Microscope. *Phys. Rev. Lett.* **1986**, *56* (9), 930−933.
(142) Rezakhaniha, R.; Agianniotis, A.; Schrauwen, J. T. C.; Griffa, A.; Sage, D.; Bouten, C. V. C.; van de Vosse, F. N.; Unser, M.; Stergiopulos, N. Experimental Investigation of Collagen Waviness and Orientation in the Arterial Adventitia Using Confocal Laser Scanning Microscopy. *Biomech. Model. Mechanobiol.* **2012**, *11* (3), 461−473.
(143) Probst, P. T.; Sekar, S.; König, T. A. F.; Formanek, P.; Decher, G.; Fery, A.; Pauly, M. Highly Oriented Nanowire Thin Films with Anisotropic Optical Properties Driven by the Simultaneous Influence of Surface Templating and Shear Forces. *ACS Appl. Mater. Interfaces* **2018**, *10* (3), 3046−3057.
(144) Magnov, S. N.; Whangbo, M.-H. Self-Assembled Structures. In *Surface Analysis with STM and AFM: Experimental and Theoretical Aspects of Image Analysis*; VCH, 1995; pp 243−276. DOI: 10.1002/9783527615117.ch12
(145) Arutyunov, P. A.; Tolstikhina, A. L. Space Surface Parameters Determined from Fourier Transforms in Atomic Force Microscopy. *Russ. Microelectron.* **2000**, *29* (6), 401−405.
(146) Xu, C.; Tian, H.; Reece, C. E.; Kelley, M. J. Topographic Power Spectral Density Study of the Effect of Surface Treatment Processes on Niobium for Superconducting Radio Frequency Accelerator Cavities. *Phys. Rev. Spec. Top.–Accel. Beams* **2012**, *15* (4), 43502.
(147) Senthilkumar, M.; Sahoo, N. K.; Thakur, S.; Tokas, R. B. Characterization of Microroughness Parameters in Gadolinium Oxide Thin Films: A Study Based on Extended Power Spectral Density Analyses. *Appl. Surf. Sci.* **2005**, *252* (5), 1608−1619.
(148) Mwema, F. M.; Akinlabi, E. T.; Oladijo, O. P. The Use of Power Spectrum Density for Surface Characterization of Thin Films. In *Photoenergy and Thin Film Materials*; Yang, X.-Y., Ed.; Scrivener Publishing, 2019; pp 379−411. DOI: 10.1002/9781119580546.ch9
(149) Jacobs, T. D. B.; Junge, T.; Pastewka, L. Quantitative Characterization of Surface Topography Using Spectral Analysis. *Surf. Topogr.: Metrol. Prop.* **2017**, *5* (1), 013001.
(150) Tosaka, M.; Murakami, S.; Poompradub, S.; Kohjiya, S.; Ikeda, Y.; Toki, S.; Sics, I.; Hsiao, B. S. Orientation and Crystallization of Natural Rubber Network As Revealed by WAXD Using Synchrotron Radiation. *Macromolecules* **2004**, *37* (9), 3299−3309.
(151) Lovell, R.; Windle, A. H. Analysis of Wide-Angle X-ray Diffraction Patterns of Aligned Glassy Polymers with Particular References to Polystyrene. *Polymer* **1976**, *17* (6), 488−494.
(152) Liu, D.; Chen, X.; Yue, Y.; Chen, M.; Wu, Q. Structure and Rheology of Nanocrystalline Cellulose. *Carbohydr. Polym.* **2011**, *84* (1), 316−322.
(153) Tatsumi, M.; Teramoto, Y.; Nishio, Y. Different Orientation Patterns of Cellulose Nanocrystal Films Prepared from Aqueous Suspensions by Shearing under Evaporation. *Cellulose* **2015**, *22* (5), 2983−2992.
(154) Song, G.; Kimura, F.; Kimura, T.; Piao, G. Orientational Distribution of Cellulose Nanocrystals in a Cellulose Whisker As Studied by Diamagnetic Anisotropy. *Macromolecules* **2013**, *46* (22), 8957−8963.
(155) Chen, S.; Schueneman, G.; Pipes, R. B.; Youngblood, J.; Moon, R. J. Effects of Crystal Orientation on Cellulose Nanocrystals−Cellulose Acetate Nanocomposite Fibers Prepared by Dry Spinning. *Biomacromolecules* **2014**, *15* (10), 3827−3835.
(156) Ureña-Benavides, E. E.; Kitchens, C. L. Wide-Angle X-ray Diffraction of Cellulose Nanocrystal−Alginate Nanocomposite Fibers. *Macromolecules* **2011**, *44* (9), 3478−3484.
(157) Rahman, M. M.; Netravali, A. N. Aligned Bacterial Cellulose Arrays as "Green" Nanofibers for Composite Materials. *ACS Macro Lett.* **2016**, *5* (9), 1070−1074.
(158) Yao, J.; Chen, S.; Chen, Y.; Wang, B.; Pei, Q.; Wang, H. Macrofibers with High Mechanical Performance Based on Aligned Bacterial Cellulose Nanofibers. *ACS Appl. Mater. Interfaces* **2017**, *9* (24), 20330−20339.
(159) Rosén, T.; Brouzet, C.; Roth, S. V.; Lundell, F.; Söderberg, L. D. Three-Dimensional Orientation of Nanofibrils in Axially Symmetric Systems Using Small-Angle X-ray Scattering. *J. Phys. Chem. C* **2018**, *122* (12), 6889−6899.
(160) Liu, P.; Zhang, Y.; Martin, S. T. Complex Refractive Indices of Thin Films of Secondary Organic Materials by Spectroscopic Ellipsometry from 220 to 1200 nm. *Environ. Sci. Technol.* **2013**, *47* (23), 13594−13601.
(161) *Structure and Properties of Oriented Polymers*, 2nd ed.; Ward, I. M., Ed.; Springer, 1997.
(162) Richard-Lacroix, M.; Pellerin, C. Orientation and Structure of Single Electrospun Nanofibers of Poly(Ethylene Terephthalate) by Confocal Raman Spectroscopy. *Macromolecules* **2012**, *45* (4), 1946−1953.

(163) Voyiatzis, G.; Petekidis, G.; Vlassopoulos, D.; Kamitsos, E. I.; Bruggeman, A. Molecular Orientation in Polyester Films Using Polarized Laser Raman and Fourier Transform Infrared Spectroscopies and X-ray Diffraction. *Macromolecules* **1996**, *29* (6), 2244−2252.
(164) Watanabe, K.; Osaka, I.; Yorozuya, S.; Akagi, K. Helically π-Stacked Thiophene-Based Copolymers with Circularly Polarized Fluorescence: High Dissymmetry Factors Enhanced by Self-Ordering in Chiral Nematic Liquid Crystal Phase. *Chem. Mater.* **2012**, *24* (6), 1011−1024.
(165) Wang, B.; Torres-Rendon, J. G.; Yu, J.; Zhang, Y.; Walther, A. Aligned Bioinspired Cellulose Nanocrystal-Based Nanocomposites with Synergetic Mechanical Properties and Improved Hygromechanical Performance. *ACS Appl. Mater. Interfaces* **2015**, *7* (8), 4595−4607.
(166) Siqueira, G.; Kokkinis, D.; Libanori, R.; Hausmann, M. K.; Gladman, A. S.; Neels, A.; Tingaut, P.; Zimmermann, T.; Lewis, J. A.; Studart, A. R. Cellulose Nanocrystal Inks for 3D Printing of Textured Cellular Architectures. *Adv. Funct. Mater.* **2017**, *27* (12), 1604619.
(167) Saha, P.; Ansari, N.; Kitchens, C. L.; Ashurst, W. R.; Davis, V. A. Microelectromechanical Systems from Aligned Cellulose Nanocrystal Films. *ACS Appl. Mater. Interfaces* **2018**, *10* (28), 24116−24123.
(168) Ureña-Benavides, E. E.; Brown, P. J.; Kitchens, C. L. Effect of Jet Stretch and Particle Load on Cellulose Nanocrystal−Alginate Nanocomposite Fibers. *Langmuir* **2010**, *26* (17), 14263−14270.
(169) Cao, L.; Cheng, Z.; Yan, M.; Chen, Y. Anisotropic Rubber Nanocomposites via Magnetic-Induced Alignment of Fe3O4/Cellulose Nanocrystals Hybrids Obtained by Templated Assembly. *Chem. Eng. J.* **2019**, *363*, 203−212.
(170) Liu, L.; Yang, X.; Yu, H.; Ma, C.; Yao, J. Biomimicking the Structure of Silk Fibers via Cellulose Nanocrystal as Beta-Sheet Crystallite. *RSC Adv.* **2014**, *4* (27), 14304−14313.
(171) He, X.; Xiao, Q.; Lu, C.; Wang, Y.; Zhang, X.; Zhao, J.; Zhang, W.; Zhang, X.; Deng, Y. Uniaxially Aligned Electrospun All-Cellulose Nanocomposite Nanofibers Reinforced with Cellulose Nanocrystals: Scaffold for Tissue Engineering. *Biomacromolecules* **2014**, *15* (2), 618−627.
(172) Sultan, S.; Mathew, A. P. 3D Printed Scaffolds with Gradient Porosity Based on a Cellulose Nanocrystal Hydrogel. *Nanoscale* **2018**, *10* (9), 4421−4431.
(173) Zhang, X.; Wang, C.; Liao, M.; Dai, L.; Tang, Y.; Zhang, H.; Coates, P.; Sefat, F.; Zheng, L.; Song, J.; Zheng, Z.; Zhao, D.; Yang, M.; Zhang, W.; Ji, P. Aligned Electrospun Cellulose Scaffolds Coated with RhBMP-2 for Both in Vitro and in Vivo Bone Tissue Engineering. *Carbohydr. Polym.* **2019**, *213*, 27−38.
(174) De France, K. J.; Badv, M.; Dorogin, J.; Siebers, E.; Panchal, V.; Babi, M.; Moran-Mirabal, J.; Lawlor, M.; Cranston, E. D.; Hoare, T. Tissue Response and Biodistribution of Injectable Cellulose Nanocrystal Composite Hydrogels. *ACS Biomater. Sci. Eng.* **2019**, *5* (5), 2235−2246.
(175) Zhao, T. H.; Parker, R. M.; Williams, C. A.; Lim, K. T. P.; Frka-Petesic, B.; Vignolini, S. Printing of Responsive Photonic Cellulose Nanocrystal Microfilm Arrays. *Adv. Funct. Mater.* **2019**, *29* (21), 1804531.
(176) Frka-Petesic, B.; Guidetti, G.; Kamita, G.; Vignolini, S. Controlling the Photonic Properties of Cholesteric Cellulose Nanocrystal Films with Magnets. *Adv. Mater.* **2017**, *29* (32), 1701469.
(177) Zhao, Y.; Gao, G.; Liu, D.; Tian, D.; Zhu, Y.; Chang, Y. Vapor Sensing with Color-Tunable Multilayered Coatings of Cellulose Nanocrystals. *Carbohydr. Polym.* **2017**, *174*, 39−47.
(178) Cherpak, V.; Korolovych, V. F.; Geryak, R.; Turiv, T.; Nepal, D.; Kelly, J.; Bunning, T. J.; Lavrentovich, O. D.; Heller, W. T.; Tsukruk, V. V. Robust Chiral Organization of Cellulose Nanocrystals in Capillary Confinement. *Nano Lett.* **2018**, *18* (11), 6770−6777.
(179) Orellana, J. L.; Wichhart, D.; Kitchens, C. L. Mechanical and Optical Properties of Polylactic Acid Films Containing Surfactant-Modified Cellulose Nanocrystals. *J. Nanomater.* **2018**, *2018*, 1−12.
(180) Mendoza-Galván, A.; Tejeda-Galán, T.; Domínguez-Gómez, A. B.; Mauricio-Sánchez, R. A.; Järrendahl, K.; Arwin, H. Linear Birefringent Films of Cellulose Nanocrystals Produced by Dip-Coating. *Nanomaterials* **2019**, *9* (1), 45.
(181) Huang, H.; Wang, X.; Yu, J.; Chen, Y.; Ji, H.; Zhang, Y.; Rehfeldt, F.; Wang, Y.; Zhang, K. Liquid-Behaviors-Assisted Fabrication of Multidimensional Birefringent Materials from Dynamic Hybrid Hydrogels. *ACS Nano* **2019**, *13* (4), 3867−3874.
(182) Chu, G.; Camposeo, A.; Vilensky, R.; Vasilyev, G.; Martin, P.; Pisignano, D.; Zussman, E. Printing Flowers? Custom-Tailored Photonic Cellulose Films with Engineered Surface Topography. *Matter* **2019**, *1* (4), 988−1000.
(183) Prathapan, R.; Glatz, B. A.; Ghosh, A. K.; Michel, S.; Fery, A.; Garnier, G.; Tabor, R. F. Enhancing Printing Resolution on Hydrophobic Polymer Surfaces Using Patterned Coatings of Cellulose Nanocrystals. *Langmuir* **2019**, *35* (22), 7155−7160.
(184) Kam, D.; Chasnitsky, M.; Nowogrodski, C.; Braslavsky, I.; Abitbol, T.; Magdassi, S.; Shoseyov, O. Direct Cryo Writing of Aerogels via 3D Printing of Aligned Cellulose Nanocrystals Inspired by the Plant Cell Wall. *Colloids Interfaces* **2019**, *3* (2), 46.
(185) Kose, O.; Boott, C. E.; Hamad, W. Y.; MacLachlan, M. J. Stimuli-Responsive Anisotropic Materials Based on Unidirectional Organization of Cellulose Nanocrystals in an Elastomer. *Macromolecules* **2019**, *52* (14), 5317−5324.
(186) Tanpichai, S.; Oksman, K. Aligned-Porous-Structured Poly(vinyl alcohol) Foams with Cellulose Nanocrystals. *AIP Conf. Proc.* **2018**, *2010*, 020007.
(187) Lu, X. Cellulose Nanocrystals for Wrinkled Fabric. *BioResources* **2019**, *14* (4), 7632−7635.
(188) Shariatzadeh, M.; Grecov, D. Aqueous Suspensions of Cellulose Nanocrystals as Water-Based Lubricants. *Cellulose* **2019**, *26* (7), 4665−4677.

https://dx.doi.org/10.1021/acsabm.0c00104
ACS Appl. Bio Mater. 2020, 3, 1828−1844